DISCLAIMER

This report was prepared as an account of work sponsored by an agency of the United States Government. Neither the United States Government nor any agency thereof, nor any of their employees, makes any warranty, express or implied, or assumes any legal liability or responsibility for the accuracy, completeness, or usefulness of any information, apparatus, product, or process disclosed, or represents that its use would not infringe privately owned rights. Reference herein to any specific commercial product, process, or service by trade name, trademark, manufacturer, or otherwise does not necessarily constitute or imply its endorsement, recommendation, or favoring by the United States Government or any agency thereof. The views and opinions of authors expressed herein do not necessarily state or reflect those of the United States Government or any agency thereof. Reference herein to any social initiative (including but not limited to Diversity, Equity, and Inclusion (DEI); Community Benefits Plans (CBP); Justice 40; etc.) is made by the Author independent of any current requirement by the United States Government and does not constitute or imply endorsement, recommendation, or support by the United States Government or any agency thereof.

Capillary Pressure to Relative Permeability

Task 7.3.4 Relative Permeability Analysis Final Report

Dr. Nathan Moodie, Ph.D.

1 EXECUTIVE SUMMARY

Surface tension affects all aspects of fluid flow in porous media. Through measurements of surface tension interaction under multiphase conditions, a relative permeability relationship can be determined. Relative permeability is a numerical description of the interplay between two or more fluids and the porous media they flow through. It is a critical parameter for various tools used to characterized subsurface multiphase flow systems, such as numerical simulation for oil and gas development, carbon sequestration, and groundwater contamination remediation. Therefore, it is critical to get a good statistic distribution of relative permeability in the porous media under study.

Empirical relationships for determining relative permeability from capillary pressure are already well established but do not provide the needed flexibility required to match laboratory derive relative permeability relationships. By expanding the existing methods for calculating relative permeability from capillary pressure data, it is possible to create both two and three-phase relative permeability relationships. Existing laboratory-measured relative permeability data along with mercury intrusion capillary (MICP) data coupled with interfacial tension and contact angle measurements were used to determine the efficacy of this approach to relative permeability curve creation. The relative permeability relationships determined with this method were fit to existing laboratory data to elucidate common fitting parameters that were then used to create relative permeability relationships from MICP data that does not have an associated laboratory-measured relative permeability relationship.

The study was undertaken as part of the Southwest Regional Partnership on Carbon Sequestration (SWP) under Award No. DE-FC26-05NT42591.

2 TABLE OF CONTENTS

3 LIST OF FIGURES

4 LIST OF TABLES

5 INTRODUCTION

Surface tension controls all aspects of fluid flow in porous media. Through careful measurements of surface tension interaction under multiphase conditions, a relative permeability relationship can be determined without expensive, time-consuming, and potentially variable relative permeability laboratory testing. Relative permeability is a numerical description of the interaction between two or more fluids as they flow through porous media. It is a critical parameter for various tools used to characterized subsurface multiphase flow systems, such as numerical simulation for oil and gas development, geologic carbon storage, and groundwater contamination remediation. Therefore it is critical to get a proper statistic distribution of relative permeability in the porous media under study. Ideally, multiple points would be sampled, and relative permeability laboratory testing would be done on those samples to build up a picture of the relative permeability relationship(s) in the reservoir of interest. However, due to the expense and time needed for this type of sampling regime relative permeability testing usually involves a minimal number of core samples taken from a limited number of points in the reservoir. Those data are then used to represent the relative permeability relationship across the entire reservoir. This could be problematic because a single point, or even a couple of points likely does not represent the heterogeneity present in the relative permeability relationship seen across the target formation. The result is a need for a robust method for determining this critical fluid/fluid/rock relationship's spatial distribution.

Empirical relationships employed to fit relative permeability and capillary pressure curves to laboratory data are already well established. Still, they are limited in their ability to leverage laboratory data to improve model resolution. Most widely used empirical relationships assume that relative permeability is between 0 and 1 for both fluids in a binary system (Brooks & Corey, 1964; Corey, 1954; van Genuchten, 1980). Laboratory testing has shown that this is usually not the case, with one or both fluids having a maximum relative permeability less than one (B. Bennion & Bachu, 2005; D. B. Bennion & Bachu, 2007; Dietrich & Bondor, 1976; Perez-Carrillo et al., 2008; Rasmussen et al., 2019; Wang, 2017). I believe that I can expand and improve on existing methods to more accurately derive relative permeability and capillary pressure simulation curves from measurements of surface tension. My method pairs measurements of interfacial tension and contact angle with capillary pressure data to calculate two- and three-phase relative permeability curves for use in numerical simulators such as Eclipse®. Ileveraged mercury intrusion capillary pressure (MICP) datasets measured on samples of the Morrow ‘B’ Sandstone. Poro-Technology measured these data under the supervision of Jason Heath, Tom Dewers, and Martha Cather as part of the SouthWest Partnership (SWP). The wettability data collected by Fan and Grigg (2015) also under the auspices of the SWP.

5.1 HYPOTHESIS

The Capillary Pressure to Relative Permeability (Pc-to-RP) method can derive an appropriate relative permeability relationship from laboratory-measured capillary pressure data. This method can create relative permeability curves for both two- and three-phase systems. It produces curves that can match laboratory measure relative permeability data or ‘up-scaled’ curves for use in reservoir simulation.

6 THEORY AND METHOD DEVELOPMENT

With the advancements in numerical simulation capabilities, highly complex multiphase, multi-physics reservoir models can be built and run efficiently. Greater heterogeneity can be added to the numerical models without worrying about the computational overhead. These advancements are conducive to adding heterogeneity in fluid/rock properties like capillary pressure and relative permeability to improve model resolution. The result is a need for a relatively quick, robust, and cost-effective method for determining the spatial distribution of these critical fluid/rock properties. Using capillary pressure data to calculate the relative permeability relationship is a promising avenue for characterizing many samples in a shorter time and for less cost than traditional relative permeability testing.

I propose a method for using relatively inexpensive and easily repeatable mercury intrusion capillary pressure (MICP) measurements coupled with wettability (surface tension) measurements and petrophysical properties (porosity and permeability) to create corresponding relative permeability relationships. Empirical relationships for determining relative permeability from capillary pressure data are already well established (Burdine, 1953; Fatt & Dykstra, 1951; Gao & Hu, 2013; Purcell, 1949) but do not provide much flexibility in specifying the critical endpoints of maximum and minimum phase saturation and in particular, the maximum phase relative permeability. I modified existing two-phase functions to allow for greater flexibility in determining these parameters and fitting the curve to laboratory relative permeability data. Using established methods, I define the critical saturation end-points from the MICP data (Engler, 2010; Honarpour et al., 2018). One essential piece of information that cannot easily be obtained from the MICP data is the maximum phase relative permeability. I explore a possible method to estimate this data developed by Swanson (1981). I then extend this method to describe three-phase fluid environments.

6.1 CALCULATING PERMEABILITY FROM CAPILLARY PRESSURE DATA

Past research has indicated that the phase permeability can be estimated from capillary pressure data. Purcell (1949) devised a method using mercury to measure capillary pressure and calculate permeability from the results. His method forced mercury through a sample of porous media under pressure. The pressure and incremental volume are recorded and plotted to create the capillary pressure curve. He derived the following empirical relationship (Equation 1) for calculating permeability from the porosity (ϕ) and the mercury capillary pressure curve based on the assumption that porous media can be modeled as a bundle of capillary tubes (Purcell, 1949).

Equation 1

$$k = \frac{(\sigma \cos\theta)^2 \tau \phi}{2} \int_{Smin}^{Smax} \frac{dS}{Pc^2}$$

With σ being the interfacial tension and θ the contact angle between mercury and air, τ the tortuosity factor, S the mercury saturation, and Pc is the mercury capillary pressure. Other authors have devised methods for determining permeability from mercury capillary pressure data, such as the Swanson method, K-T method, and the Gao method (Gao & Hu, 2013; Katz & Thompson, 1987; Swanson, 1981; Webb, 2001). These formulas and procedures may also prove useful for investigating the relationship between laboratory data and empirical formulas.

6.2 RELATIVE PERMEABILITIES FROM CAPILLARY PRESSURE DATA

Expanding on Purcell's formula for calculating permeability from capillary pressure experiments, Fatt & Dykstra (1951) and Burdine (1953) both derive similar equations for calculating wetting phase relative permeability from capillary pressure/saturation data. For my method, I use the Fatt & Dykstra (1951) derivation for the wetting phase relative permeability (Equation 2).

Equation 2

$$k_r = \frac{\int_0^s \frac{dS}{Pc^{2(1+b)}}}{\int_0^{100} \frac{dS}{Pc^{2(1+b)}}}$$

With *S* being the wetting phase saturation, *Pc* the capillary pressure of the wetting phase, and *b* a constant that defines the shape of the resulting curve.

6.3 THEORY AND DERIVATION

My theory and derivation follow closely work done by Fatt and Dykstra (1951), Purcell (1949), and Burdine (1953). I assume that the total flow rate through porous media can be approximated by the flow through a bundle of capillary tubes (1).

(1)

$$Q_t = \sum_{i=1}^{N} Q_i$$

The flow rate through a single capillary tube can be approximated by Poiseuille's Law (2),

(2)

$$\Delta P = \frac{8\mu l Q}{\pi r^4}$$

where μ is the fluid viscosity, Δ*P* is the pressure differential across the capillary tube of length *l,* and radius *r* with a fluid viscosity of μ. It is assumed that the capillary tube length *l* is equivalent to the fluid path length and that Darcy's Law (3) applies for laminar flow of an incompressible fluid through a porous media,

(3)

$$Q = \frac{kA\Delta P}{\mu L}$$

where *k* is the permeability and Δ*P* is the pressure differential of a fluid with μ viscosity across a sample of area *A* and length *L*. Rearranging (2) in terms of *Q* and then substituting Darcy's Law (3) for *Q* gives the following formula in terms of permeability,

(4)

$$k = \frac{\pi r^4 L}{8Al}$$

The volume of a capillary tube is given as,

(5)

$$V = \pi r^2 l$$

where *V* is the pore volume. Rearranging (5) in terms of π and substitute into (4) to get the volume term, giving the following relationship,

(6)

$$k = \frac{r^2 LV}{8Al^2}$$

Next, I relate saturation to volume in a porous media by,

(7)

$$S = \frac{V}{\phi AL}$$

where ϕ is the porosity. Rearranging (7) in terms of volume and substituted into (6) gives the following relationship,

(8)

$$k = \frac{\phi r^2 L^2 S}{8l^2}$$

Tortuosity (τ) is introduced to account for the fact that in a porous media, the fluid flow path length *l* is longer than the sample length *L* and is assumed to be inversely related to the pore radius by,

(9)

$$\tau = \frac{l}{L} = \frac{a}{r^b}$$

where *a* and *b* are constants defined by the porous media. Substituting (9) into (8) gives the following equation in terms of pore radius,

(10)

$$k = \frac{\phi r^{2(1+b)} S}{8a^2}$$

The following formula relates capillary pressure to pore radius and wettability,

(11)

$$Pc = \frac{2\sigma cos\theta}{r}$$

where σ is the interfacial tension, and θ is the contact angle between the wetting and non-wetting fluid phases. Rearranging (11) in terms of pore radius and substituting into (10) gives the following relationship for a single capillary tube,

(12)

$$k = \frac{\phi(2\sigma cos\theta)^{2(1+b)}S}{8a^2 Pc^{2(1+b)}}$$

Assume *a* and *b* are constant, for a bundle of *N* capillary tubes (12) becomes (13).

(13)

$$k = \frac{\phi(2\sigma cos\theta)^{2(1+b)}}{8a^2}\sum_{i=1}^{N}\frac{\partial S_i}{Pc_i^{2(1+b)}}$$

To this point, I have followed the derivation done by Fatt and Dykstra (1951). I now modified this relationship by parameterizing the saturation endpoints of the integral form of (13) to span from the residual wetting phase saturation (S_{wr}) to the maximum wetting phase saturation (S_{max}) (14). I now have greater flexibility in how the saturation endpoints are defined and fitting the calculated relative permeability curves to laboratory data. This data rarely spans the entire saturation range, generally spanning from a residual wetting phase saturation to a maximum wetting phase saturation that can be less than 100% (B. Bennion & Bachu, 2005; Chen et al., 2014; S. C. M. Krevor et al., 2012; Oak et al., 1990; Rasmussen, et al., 2019; Wang, 2017; Ward & Morrow, 1987). If I integrate over the saturation range of S_{wr} to S_{max} I get a measure of the permeability of the sample.

(14)

$$k = \frac{\phi(2\sigma cos\theta)^{2(1+b)}}{8a^2}\int_{S_{wr}}^{S_{max}}\frac{\partial S_w}{Pc^{2(1+b)}}$$

If I integrate over the saturation range of S_{wr} to S_w I get a measure of the effective permeability at S_w.

(15)

$$k_e = \frac{\phi(2\sigma cos\theta)^{2(1+b)}}{8a^2}\int_{S_{wr}}^{S_w}\frac{\partial S_w}{Pc^{2(1+b)}}$$

Relative permeability k_r is related to permeability k (14) and effective permeability k_e (15) by,

(16)

$$k_r = \frac{k_e}{k}$$

Substituting (14) and (15) into (16) gives the following formula for wetting phase relative permeability k_{rw},

(17)

$$k_{rw} = \frac{\int_{S_{wr}}^{S_w}\frac{dS_w}{P_c^{2+2b}}}{\int_{S_{wr}}^{S_{max}}\frac{dS_w}{P_c^{2+2b}}}$$

Here, I extend the work of Fatt and Dyskra (1951), Burdine (1953), and Purcell (1949) to the non-wetting phase relative permeability k_{rn}. I change the saturation range in (15) to span the interval from the S_w to the S_{max}. This represents the change in the non-wetting phase saturation and, when substituted into (16), give the non-wetting phase relative permeability k_{rn}.

(18)

$$k_{rn} = \frac{\int_{S_w}^{S_{max}} \frac{dS_w}{P_c^{2+2b}}}{\int_{S_{rw}}^{S_{max}} \frac{dS_w}{P_c^{2+2b}}}$$

Now I have formulas for calculating both the wetting and non-wetting relative permeability from capillary pressure measurements. To generate relative permeability curves from laboratory capillary pressure data, I use the trapezoidal rule to approximate the integration and make the formula useable for discrete data.

(19)

$$k_{rw} = k_{w\,max} * \left(\frac{S_w - S_{wr}}{S_w^{max} - S_{wr}}\right)^c * \frac{\left(\frac{S_{wr}}{Pc(S_{wr})^{2+2b}} + \frac{S_w}{Pc(S_w)^{2+2b}}\right)}{\left(\frac{S_{wr}}{Pc(S_{wr})^{2+2b}} + \frac{S_w^{max}}{Pc(S_w^{max})^{2+2b}}\right)}$$

(20)

$$k_{rn} = k_{n\,max} * \left(\frac{S_w^{max} - S_w}{S_w^{max} - S_{wr}}\right)^c * \frac{\left(\frac{S_w}{Pc(S_w)^{2+2b}} + \frac{S_w^{max}}{Pc(S_w^{max})^{2+2b}}\right)}{\left(\frac{S_{wr}}{Pc(S_{wr})^{2+2b}} + \frac{S_w^{max}}{Pc(S_w^{max})^{2+2b}}\right)}$$

The exponent *c* in the effective saturation term is introduced in place of the '*2*' as a fitting parameter to allow greater flexibility in fitting to laboratory data. The exponents *b* and *c* can be derived by fitting the curves to laboratory data or using literature values. See section *7.3 Relative Permeability Data and Endpoints* for more details.

6.4 Capillary Pressure to Relative Permeability (Pc-to-RP) Method

I propose the following method for determining a relative permeability relationship for either a two-phase or three-phase fluid system from Mercury Intrusion Capillary Pressure (MICP) data and the appropriate wettability data. I will show the detailed steps for determining a two-phase relationship and then discuss the modification needed to determine the curves for a three-phase system.

6.4.1 Two-Phase System

1) First, I must determine the saturation endpoints (S_w max and S_w min). When I graph the capillary pressure versus wetting phase saturation, there are two inflection points on the graph representing the

residual wetting and non-wetting phase saturations. I find these by plotting the capillary pressure versus 1 - Hg saturation data from the MICP tests.[1]

a) The non-wetting phase residual saturation is found by observing the inflection point corresponding to the change in the slope from convex to concave that happens during initial non-wetting phased intrusion into the sample (labeled S_{nr} in Figure 1 and corresponding the $S_w max$ in Equation 3 and Equation 4). This change in slope is most easily found by calculating the 2nd derivative of the capillary pressure data and observing the change in sign for negative to positive.

b) The wetting-phase residual saturation is not as easy to determine. This value is traditionally associated with the point on the graph where it goes to nearly vertical, indicating no more mercury can be intruded into the microscopic pores and thus reaching wetting phase residual saturation, S_{wr} in Figure 1 (Engler, 2010; Honarpour, et al., 2018). Laboratory measured relative permeability done both by the SWP (Rasmussen, et al., 2019; Wang, 2017) and from the literature indicate that the wetting phase residual saturation corresponds with the point labeled S_{wcrit} in Figure 1 (B. Bennion & Bachu, 2005, 2006; S. C. Krevor et al., 2011; S. C. M. Krevor, et al., 2012). To find this point take the first derivative of the capillary pressure and find the greatest change in the angle between successive pressure steps. This point is assumed to be the minimum wetting phase saturation ($S_w min$ in Equation 3 and Equation 4) for the relative permeability relationship.

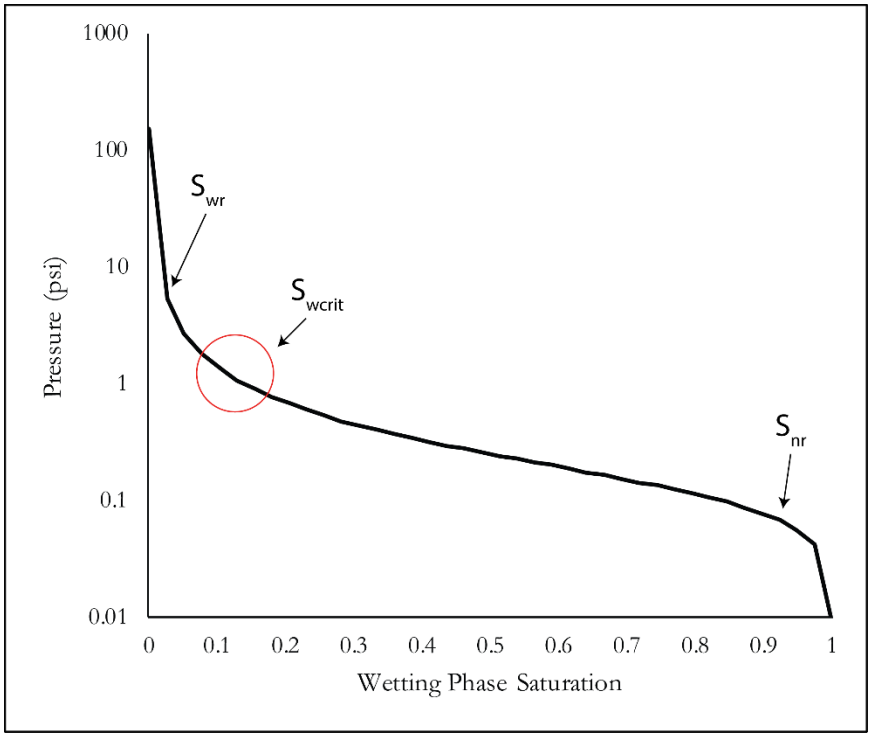

Figure 1 Inflection points on the water saturation versus pressure graph are used to determine the residual wetting phase (S_{rw}), critical wetting phase saturation (S_{wcrit}), and non-wetting phase (S_{rn}) saturation endpoints.

2) I now need to find the intrinsic permeability (k) and the effective phase permeability (k_{ew} and k_{en}). I calculate the permeability at each pressure/Hg saturation step by applying Purcell's formula (Equation

[1] For other types of capillary pressure data, I plot the pressure versus the wetting phase saturation. The data can be plotted as pressure versus Hg saturation (non-wetting), but I find it easier to analyze when it is plotted against the wetting phase saturation.

1) with the appropriate interfacial tension (γ) and contact angle (θ) parameters. The maximum value calculated is assumed to be the intrinsic permeability of the sample (k).

a) The wetting phase effective permeability (k_{ew}) is calculated by applying Equation 1 over the interval from $S_{Hg}=S_w max$ to $S_{Hg}max=1$. I assume that the maximum permeability of the sample to the wetting phase (k_{ew}) can be calculated from the point of maximum wetting phase saturation. This assumes that any wetting phase fluid that imbibes into the very small pores will not contribute significantly to fluid flow, thus reaching the point of maximum wetting-phase fluid flow and thus maximum wetting-phase permeability.

b) The non-wetting phase effective permeability (k_{en}) is calculated by applying Equation 1 over the interval from $S_{Hg}=[S_{Hg}@45°]$ to $S_{Hg}max=1$. According to Swanson (1981) the bulk fluid flowing through the majority of the pore space is where that angle of the 1st derivative of the capillary pressure data equals 45 degrees. He assumed this to be a measure of the effective permeability of the sample. I use this point as the effective non-wetting permeability under the assumption that it accounts for both wetting and non-wetting phase residual saturations.

3) The relative permeability endpoint can be determined by dividing the effective phase permeability calculated in 2a) and 2b) by the intrinsic permeability calculated in 2) (k_{ew}/k and k_{en}/k). If the effective phase permeability (k_e) is larger than the intrinsic permeability (k) it is assumed that the maximum phase relative permeability endpoint is 1. Determining the maximum phase relative permeability is critical for accurately creating relative permeability relationships from capillary pressure data but also the most uncertain.

4) Now that I know all the critical endpoints, the next step is to calculate the relative permeability curves. The formula for the wetting phase is Equation 3 and for the non-wetting phase is Equation 4. Both the b exponent and c exponent are defined independently for the wetting and non-wetting curves. See section *7.3 Relative Permeability Data and Endpoints* below for a detailed description of the fitting parameters used.

Equation 3

$$k_{rw} = k_{w\,max} * \left(\frac{S_w - S_{wr}}{S_w^{max} - S_{wr}}\right)^c * \frac{\left(\frac{S_{wr}}{Pc(S_{wr})^{2+2b}} + \frac{S_w}{Pc(S_w)^{2+2b}}\right)}{\left(\frac{S_{wr}}{Pc(S_{wr})^{2+2b}} + \frac{S_w^{max}}{Pc(S_w^{max})^{2+2b}}\right)}$$

Equation 4

$$k_{rn} = k_{n\,max} * \left(\frac{S_w^{max} - S_w}{S_w^{max} - S_{wr}}\right)^c * \frac{\left(\frac{S_w}{Pc(S_w)^{2+2b}} + \frac{S_w^{max}}{Pc(S_w^{max})^{2+2b}}\right)}{\left(\frac{S_{wr}}{Pc(S_{wr})^{2+2b}} + \frac{S_w^{max}}{Pc(S_w^{max})^{2+2b}}\right)}$$

6.4.2 Three-phase system

To use this method to calculate three-phase relative permeability relationships, I assume that a three-phase relationship can be described by two fluid pairs, oil/water and gas/oil (or CO_2/oil), and the use of a combination model, such as the Stone I, Stone II or the Baker model (Baker, 1988; Stone, 1970, 1973). Most numerical simulators make this assumption, and thus calculating relative permeability as binary pairs in a ternary system has the advantage of being directly portable to numerical simulation.

1) Determine the saturation endpoints from the MICP data is the first step in the method. I need to determine four endpoints; the oil/water wetting and non-wetting residual/critical saturations and the gas/oil wetting and non-wetting residual/critical saturations. The oil/water endpoints need to be

determined first. The steps are the same as in the two-phase method outlined above and will not be repeated here.

a) The saturation endpoints ($S_l$max and $S_l$min) for the gas/oil relative permeability relationship are determined from the endpoints identified for the oil/water relationship. The liquid phase (residual water plus oil) maximum saturation value is set to the maximum wetting phase value ($S_w$max) from the oil/water relationship. This value would correspond to the residual gas saturation.

b) The minimum liquid saturation value ($S_l$min) is set to 1-$S_w$min-(1-$S_w$max). This is done for the Eclipse numerical simulator requirements for the SGOF and SWOF keywords. If this is not a requirement, then the same method used for $S_w$min can be used.

2) Similar to the steps taken in the two-phase method, the effective permeability for each fluid pair is determined at each pressure/Hg saturation step by applying Purcell's formula (Equation 1) with the appropriate interfacial tension (γ) and contact angle (θ) parameters. For a three-phase system, the effective permeability is calculated separately for the gas/oil relationship and the oil/water relationship. There are four points in this data that are critical to identify, effective permeability to water (k_{ew}), effective permeability to oil in the oil/water relationship (k_{eow}), effective permeability to gas (k_{eg}), and effective permeability to oil in the gas/oil relationship (k_{eog}).

   a) The first critical point is the permeability at the water phase residual saturation ($S_w min$). I identify this point as the effective water phase permeability (k_{ew}).

   b) The second critical point represents the permeability of the sample that corresponds to when the angles of the 1st derivative of the capillary pressure versus Hg saturation curve is equal to 45 degrees (Swanson, 1981).[2] This point is identified as the effective oil phase permeability (k_{eow}) for the oil/water fluid pair.

   c) The third critical point is the effective permeability to oil (k_{eog}) in the gas/oil fluid pair. This point corresponds to the residual gas saturation ($S_l max$) point. This point is chosen because at $S_l max$ the only fluid flowing is oil and is assumed to be the maximum permeability to the oil phase (k_{eog}).

   d) The fourth critical point is the effective permeability to gas (k_{eg}) in the gas/oil fluid pair. This point is determined the same way as the k_{eow} point in step 2b) but using the gas/oil effective permeability data.

3) The relative permeability endpoints can now be determined. The wetting and non-wetting phase relative permeability endpoint are determined by $k_r max = k_e/k$. If k_e is larger than k it is assumed that the relative permeability endpoint ($k_r max$) is 1. Applying the k and k_e calculated in 2), I determine the four critical points, $k_{rw} max$ and $k_{row} max$ for the oil/water relationship and $k_{rg} max$ and $k_{rog} max$ for the gas/oil relationship.[3]

---

[2] Under some circumstances (shale/limestone samples), the 1st derivative of the capillary pressure is greater than 45 degrees for all pressure steps. In this case, further study is required to determine the proper approach for determining this end-point.

[3] Eclipse simulator requires the maximum relative permeability for the oil in the oil/water ($k_{row} max$) and gas/oil ($k_{rog} max$) relationships must be the same value. When this value is calculated it is different for each of the fluid pairs. Experimental relative permeability testing by the SWP indicates a value between 0.8 to 1 for the maximum relative permeability of oil in both the oil/water and gas/oil fluid pairs over the five tests conducted (Rasmussen, et al., 2019; Wang, 2017).

4) All critical endpoints have now been determined. The relative permeability curves can be calculated using Equation 3 and Equation 4.

    a) Like the two-phase method, the exponents *b* and *c* are used to determine the shape of the relative permeability curve. They are defined independently for the wetting and non-wetting phases.

7 LABORATORY DATA AND METHOD PARAMETERS

The SWP collected laboratory data on samples from the Farnsworth Unit (FWU) in the northeast Texas Panhandle, the site of an active CO_2-EOR operation. The target formation is the Morrow 'B' Sandstone, a clastic formation composed of medium to coarse sands that is overlain by a thick shale deposit and capped by the Thirteen Finger Limestone. Samples from both the reservoir and the overlying units have been measured for capillary pressure, relative permeability, and wettability. The following is a brief summary of the data collected and its use in this method's development.

7.1 MERCURY INTRUSION CAPILLARY PRESSURE DATA

The SWP measured capillary pressure using mercury intrusion capillary pressure (MICP) testing on 39 core samples from three wells within the FWU, two on the west-half (13-10A and 13-14) and one on the east-half of the field (32-8). The samples are from the overlying Thirteen Finger Limestone and Morrow Shale, the Morrow 'B' Sandstone, and the Morrow 'B1' Base. For this study, I chose to use only the 22 samples from the west-half of the field, wells 13-10A and 13-14, because that is the area of ongoing field operations and the domain of the geological model.

7.1.1 MICP closure corrections

Before I can use the MICP data, the closure corrections initially estimated during testing needs to be checked and updated if necessary. The closure correction corrects for the volume of mercury that fills the space between the core sample and the injection-plate. It is needed when calculating the permeability using Swanson's equations (Equation 5 and Equation 6). The MICP closure corrections were initially evaluated by the testing laboratory before I received the data. I double-checked the closure corrections and modified values as necessary according to Equation 5 and Equation 6 (Swanson, 1978).

Equation 5

$$\frac{S_b}{Pc} = \frac{\left(V_c - \left[\frac{CC * W_s * 100}{BV}\right]\right)}{Pres_{inlet}}$$

where V_c is the cumulative volume intruded into the sample, CC is the closure correction, W_s is the sample weight, BV is the sample bulk volume, and $Pres_{inlet}$ is the inlet pressure.

Equation 6

$$Perm_{Sw} = 399 * Max\left(\sum_{i}^{n=1} \frac{S_b}{Pc}\right)^{1.691}$$

7.1.2 Classifying the MICP data into Hydrostratigraphic Unit (HU)

For this study, I want to classify the MICP data according to the hydrostratigraphic unit framework that the SWP has been developing throughout the project. I apply the Winland R35 method (Equation 8) to classify hydrostratigraphic unit (HU) across the sampled interval according to the method used by Rose-Coss et al. (2016) and Aguilera and Aguilera (2001). Twenty-two samples were classified into their respective HU by the cut-offs specified in Table 1 from Rose-Coss et al. (2016). Of those samples, 16 are from the Morrow 'B' Sandstone, and the remaining 6 are from the overlying and underlying formations. The Morrow 'B' Sandstone is classified from HU1 to HU8 as the porosity and permeability increase. The overlying Morrow Shale and the underlying Morrow Shale formation down to the Morrow 'D' unit are

assigned a 'shale' HU, and the deeper Morrow 'D' unit's HUs were assigned using Equation 8. Table 1 lists the HU calculated for each sample.

Equation 7

$$Log\ R35 = 0.732 + 0.588 * logk_{air} - 0.864 * log\phi_{core}$$

Equation 8

$$r35 = 5.395 * \left(k^{0.588}/_{\phi^{0.864}}\right)$$

I would like to address a terminology difference between my work and that of Rose-Coss et al. (2016) concerning *hydrostratigraphic units* versus *hydraulic flow units*. In Rose-Coss et al. (2016) the authors refer to hydrogeologic units that have similar flow properties and geology but are distinct from nearby units as Hydraulic Flow Units or HFUs. This is terminology based on work done by Amaefule et al. (1993), Svirsky et al. (2004), and others related to oil and gas exploration (Abbaszadeh et al., 1996; Aguilera & Aguilera, 2001). Previous to their work Maxey (1964) described the same type of hydrogeologic units but under a framework relating to groundwater aquifers. He states:

> "In order to crystallize meanings, to set apart clearly these geohydrologic units from lithologic or other units, and to clarify usage in applications of hydrogeologic knowledge to water problems, it is *proposed that a category of hydrostratigraphic units* be recognized, these units to be defined as 'bodies of rock with considerable lateral extent that compose a geologic framework for a reasonable distinct hydrologic system'" (Maxey, 1964).

I believe that both of these terminologies are describing the same thing, a unit of rock with similar hydrological and lithological properties that is distinct from surrounding units of similar lithology but differing hydrology. The term 'hydraulic flow' unit only captures the flow aspect of the hydrogeology and thus is not an accurate term to describe what is being measured. For the remainder of this report, I will use the term hydrostratigraphic unit in place of hydraulic flow unit.

Table 1. Hydrostratigraphic Unit classification cut-off values from the study done by Rose-Cross et al. (2016) on core samples taken from the FWU.

Hydrostratigraphic Unit	*R35 (μ) Bin*	*Pore Throat Size Classification*	*Pore Type*	*Description*
HU1	> 0.65	Micro	Predominantly intragranular micro porosity	Intergranular porosity occluded by calcite of siderite cement
HU2	0.66 - 1.04	Meso	Predominantly intragranular micro porosity	Porosity, when present, comes from authogenic kaolinite replacing feldspar
HU3	1.05 - 1.86	Macro	Intragranular micro and a greater amount of intragranular macro porosity as well as sparse intergranular micro and macro porosity	Higher degree of grain dissolution leads to grater porosity. Intergranular porosity low due to dispersed detrital clay and calcite or siderite cement.
HU4	1.87 - 2.96	Macro	Intermediate between HSU3 and HSU5	More or less intergranular porosity leads to some connection of pore throats

HU5	2.97 - 3.69	Macro	Intragranular micro and macro porosity as well as intergranular micro and macro porosity.	Lack of cementation and varying degrees of grain dissolution can create interconnected pore networks.
HU6	3.7 - 5-95	Macro	Intragranular micro and macro porosity as well as intergranular micro and macro porosity.	Intermediate between HSU5 and HSU 8
HU7	5.96 - 9.35	Macro	Intragranular micro and macro porosity as well as intergranular micro and macro porosity.	Intermediate between HSU5 and HSU 8
HU8	< 9.5	Mega	Intragranular micro and macro porosity, intergranular macro porosity	Complete grain dissolution lack of cementation, and poor sorting create mega pore spaces, and larger pore throats.

Table 2. MICP samples correlated to the calculated hydrostratigraphic unit.

MICP Samples Correlated to Hydrostratigraphic Units					
Well	*ID*	*Sample Depth(ft)*	*Log R35 (μ)*	*HU*	*Formation*
13-10A	54	7673.7	3.2348	5	Morrow 'B' Sandstone
13-10A	56	7687.8	9.5520	8	Morrow 'B' Sandstone
13-10A	58	7691.21	4.2507	6	Morrow 'B' Sandstone
13-10A	60	7701.05	13.3532	8	Morrow 'B' Sandstone
13-10A	E1	7675.9	2.0954	4	Morrow 'B' Sandstone
13-10A	E2	7684.75	1.1030	3	Morrow 'B' Sandstone
13-10A	E3	7686.4	1.4960	3	Morrow 'B' Sandstone
13-10A	E4	7696.25	3.6392	5	Morrow 'B' Sandstone
13-10A	E6	7668.1	0.0089	Shale	Morrow Shale
13-14	41T	7617.26	0.0022	Shale	Thirteen Fingers Limestone
13-14	45S	7681.28	0.0018	Shale	Morrow Shale
13-14	48M	7700.51	0.0202	1	Morrow 'B' Sandstone
13-14	49	7701.67	2.6821	4	Morrow 'B' Sandstone
13-14	50	7701.79	0.7934	2	Morrow 'B' Sandstone
13-14	52	7735.2	0.0078	Shale	Morrow 'B1' Base
13-10A	53M	7673.7	0.8611	2	Morrow 'B' Sandstone
13-10A	55	7687.8	5.8748	6	Morrow 'B' Sandstone
13-10A	57	7691.21	3.1280	5	Morrow 'B' Sandstone
13-10A	59	7701.05	10.6626	8	Morrow 'B' Sandstone
13-10A	70 V	7523.95	0.0000	Limestone	Thirteen Finger Limestone
13-10A	78 V	7633.76	0.0036	Shale	Morrow Shale
13-10A	82 V	7685.25	0.1608	1	Morrow 'B' Sandstone

7.2 WETTABILITY DATA

7.2.1 Contact Angel

The contact angle is a critical piece of data needed to convert the MICP data from a mercury/air fluid pair to oil/water and gas/oil fluid pairs at reservoir conditions using Equation 9. Laboratory data for both oil in brine and brine in oil contact angles have been measured by Fan and Grigg (2015) for the Morrow 'B' Sandstone at Farnsworth. These tests provide data in both a water-wet and an oil-wet system and indicate that the Morrow 'B' Sandstone is likely a water-wet system. A contact angle of 24.7° between the oil drop in brine compared to the contact angle of 106.5° for the brine drop in oil indicates that the water has a stronger surface adhesion and wetting capacity. This reinforces the assumption of a water-wet system due to the extensive water-flooding started in the 1960s and continuing today. In addition to the measured contact angle data, a mixed-wet system was explored using a value of 89°, see Table 3 for the oil/water contact angle data.

Equation 9

$$P_{c(brine/CO_2)} = P_{c(air/Hg)} \frac{\gamma_{(brine/CO_2)} * \cos\theta_{brine/CO_2}}{\gamma_{(air/Hg)} * \cos\theta_{(air/Hg)}}$$

The contact angle for the CO_2/oil system has not been measured at Farnsworth. I Assume that even at full miscibility, the oil and residual brine will become saturated with CO_2, and a separate supercritical phase will form. It is not thought that the CO_2 wets the Morrow 'B' Sandstone, but testing would need to be done to address this assumption. Under the assumption of a strongly fluid-wet system, oil plus residual water, I use a very shallow contact angle of 5° for the gas/oil system.

Table 3 Contact angle data used in the method development. Water-wet contact angel is oil in a brine-flooded core, and the oil-wet contact angle is water in an oil-flooded core (Fan & Grigg, 2015).

Laboratory Contact Angle Data		
Water-Wet	24.7°	+- 3.1°
Oil-Wet	106.5°	+- 4.4°
Mixed-Wet	89°	

7.2.2 Interfacial Tension

The reservoir pressure at Farnsworth is roughly 4500 psi (31 MPa), well above the bubble point or minimum miscibility pressure (MMP) of the reservoir. Laboratory studies have indicated that as gas reaches its MMP in oil, the interfacial tension (IFT) approaches zero (Gasem et al., 1993; Hemmati-Sarapardeh et al., 2013; Yang & Gu, 2005; Yang et al., 2005). Above the MMP, the IFT is assumed to be zero as the gas should all be dissolved in the oil. According to work done by Yang et al. (2005) the interfacial tension between CO_2 and oil at the maximum pressure tested (16.11 MPa) is about 1.5 dyne/cm. As the pressure increased from 8.87 MPa to 16.11 MPa they saw a small decrease in interfacial tension of 1.5 dyne/cm (Yang, et al., 2005). Hemmati-Sarapardeh et al. (2013) measured IFT for crude oil and CO_2 under a variety of pressure and temperature conditions with similar results. At 100°C, the highest temperature tested, the interfacial tension decreased linearly with increasing pressure from about 10 MPa to just under 20 MPa. Rosman and Zana (1977) measured an interfacial tension of 0.105 dyne/cm at 15.2 MPa and 54.4°C and 0.03 dyne/cm at 16 MPa and 54.4°C for a solution of 55% mole CO_2 in oil. Gasem et al. (1993) measured interfacial tension in CO_2 and reservoir oil at 54.4°C that dropped from 1.23

dyne/cm at 11.7MPa to 0.007 dyne/cm at 16.8 MPa. From their experiments, the interfacial tension appears to asymptotically approach zero as the pressure reaches the bubble point, never reaching zero.

If this data is extrapolated to the pressures (31 MPa) and temperatures (71°C) at Farnsworth, then according to the previous work, the interfacial tension should be zero. But work done by Yang and Gu (2004) cast some doubt on that claim by showing incomplete miscibility of CO_2 in the oil phase well above the MMP. They showed that at 28.3 MPa and 58°C, the interfacial tension stabilizes between 1 and 2 dyne/cm, never approaches zero, or ultra-low number (Yang & Gu, 2005). In their experiments, full miscibility was not achieved with the oil, even after multiple contacts (Yang & Gu, 2005; Yang, et al., 2005). They attribute this behavior to the CO_2 extracting the light oil components until only the heavy components are left in the oil phase, and at this point, the fluids reach a stable equilibrium interfacial tension (Yang & Gu, 2005).

Under the high temperature and pressure conditions at the Farnsworth Unit, it has been assumed that the CO_2 is fully miscible in the oil, and there is no interfacial tension. But the work cited above indicates that even under these conditions, there should be a small interfacial tension between the CO_2 and oil. Since there is no measured interfacial tension for the Farnsworth Unit for CO_2 and oil, I assume a small value of 0.27 dyne/cm for the gas/oil IFT based on the studies cited above.

Unlike the CO_2/oil fluid pair, the oil and water are not miscible at the temperature and pressure conditions at the Farnsworth Unit, and assuming a low or zero IFT is not accurate for the fluid system. I used 13.7 dyne/cm for the oil/water interfacial tension based on extrapolating work done by other researchers to the pressure and temperature conditions at the FWU. Studies that have measured oil/water interfacial tension are generally at lower temperatures and pressures than present at the FWU and indicate values of between 18 and 35 dyne/cm depending on the testing conditions and fluid makeup (Firoozabadi & Ramey Jr, 1988; Hocott, 1939; McCaffery, 1972; Morrow, 1990; Yang, et al., 2005). It has been found that as the pressure increase, there is a slight increase in the interfacial tension, but as you increase temperature, there is a much larger decrease in interfacial tension. If you extrapolate this trend, then an IFT of 13.7 dyne/cm makes sense for the conditions observed.

7.2.3 Water-wet parameters and discussion

The interfacial tension and contact angle values in Table 4 describes a strongly water-wet system thought to exist currently at the FWU.

Table 4. Wettability Data used to describe a water-wet three-phase fluid system.

Water-wet		
	Interfacial Tension γ (dyne/cm)	*Contact Angle (θ)*
Gas/Oil	0.27	5
Oil/Water	13.7	24.7
Mercury/Air	485	40

7.2.4 Oil-Wet parameters and discussion

The interfacial tension and contact angle in Table 5 describe a weakly oil-wet system that may have been present before water-flooding operations started at the Farnsworth Unit. It is not thought that the reservoir is currently oil-wet, but it is useful to study how changing the wettability of the fluid system used to develop the relative permeability and capillary pressure relationships affects the numerical simulations.

Table 5. Wettability Data used to develop the oil-wet relative permeability and capillary pressure curves using the Pc-to-RP curve creation method.

Oil-wet		
	Interfacial Tension γ (dyn/cm)	*Contact Angle (θ)*
Gas/Oil	0.27	5
Oil/Water	13.7	106.5
Mercury/Air	485	40

7.2.5 Mixed-wet parameters and discussion

The interfacial tension and contact angle in Table 6 describe a mixed-wet fluid system at the FWU. Engineers on the SWP project have described the wettability as mixed to water-wet. For this study, I also wanted to evaluate a mixed-wet system and used 89° for the contact angle to describe that system.

Table 6. Wettability Data used for the mixed-wet Pc-to-RP curve creation.

Mixed-wet		
	Interfacial Tension γ (dyne/cm)	*Contact Angle (θ)*
Gas/Oil	0.27	5
Oil/Water	13.7	89
Mercury/Air	485	40

7.3 Relative Permeability Data and Endpoints

7.3.1 Two-phase data

Laboratory data measured by Bennion and Bachu (2005, 2006) and Krevor et al. (2011; 2012) had both the capillary pressure data and relative permeability data, making a perfect candidate for this analysis. Bennion and Bachu (2005, 2006) measure six samples from various potential sandstone and carbonate reservoir rock. Krevor et al. (2011, 2012) measured four samples of potential sandstone reservoirs. I have ten sets of relative permeability and capillary pressure data to use in my method development between these two studies. I digitize the data from their papers and plot it in Excel® so I can extract the maximum wetting and non-wetting phase relative permeability and the residual wetting and non-wetting phase saturations. See Table 7 for the critical end-points and Appendix I Figure 18 to Figure 27 for the relative permeability and capillary pressure data and fit curves.

Table 7 Critical end-points derived from laboratory-measured relative permeability and capillary pressure data.

Sample Name Author(s)	**Basal Cambrian Sandstone** Bennion (2005, 2006)	**Wabamun - low perm** Bennion (2005, 2006)	**Ellerslie Sandstone** Bennion (2005, 2006)	**Viking Sandstone** Bennion (2005, 2006)	**Cooking Lake Carbonate** Bennion (2005, 2006)
k_{rw}**max**	0.951	1.000	1.000	1.000	1.000
k_{rn}**max**	0.658	0.529	0.115	0.331	0.068
S_{wr}	0.300	0.595	0.659	0.556	0.476
S_{nr}	0.000	0.000	0.000	0.000	0.000

Sample Name **Author(s)**	**Nisku Carbonate** Bennion (2005, 2006)	**Berea Sandstone** Krevor (2011, 2012)	**Mt Simon Sandstone** Krevor (2011, 2012)	**Paaratte Sandstone** Krevor (2011, 2012)	**Tuscaloosa Sandstone** Krevor (2011, 2012)
k_{rw}**max**	1.000	0.998	0.999	1.000	1.000
k_{rn}**max**	0.175	0.380	0.460	0.301	0.050
S_{wr}	0.331	0.454	0.460	0.410	0.794
S_{nr}	0.000	0.002	0.001	0.000	0.000

7.3.2 Three-phase data

The SWP has a suite of 17 laboratory-measured two-phase relative permeability relationships for the Morrow "B" Sandstone, nine oil/water tests and nine gas/oil tests. The oil/water data consists of nine relative permeability curves measured on nine different core samples, two measured by the China University Petroleum Beijing (CUPB), one by UNOCAL, and six by Rasmussen et al. (2019) (Table 8). The CO_2/oil data consists of eight relative permeability curves measured on four different core samples, one by CUPB, one by UNOCAL, and six by Rasmussen et al. (2019) on two core samples at different pressures.

I digitize the data from Wang (2017) and plot it in Excel® and data shared with me by Rasmussen et al. (2019). The extracted maximum wetting and non-wetting phase relative permeability and the residual wetting and non-wetting phase saturations are in Table 8. See Appendix 1 Figure 28 to Figure 32 for plots of the curves.

*Table 8. Oil/water relative permeability critical points derived from laboratory data. *May (1988) indicates that the data was changed to make it 'simulator ready'.*

	Sample 5-1	*Sample 3-9*	*UNOCAL*	*Core 19 (HU 5)*	*Core L7 (HU 4)*	*Core L6 (HU 3)*	*Core L5 (HU 3)*	*Core L4 (HU 2)*	*Core 1 (HU 1)*
k_{rw}**max**	0.147	0.148	0.270	0.091	0.215	0.186	0.102	0.166	0.183
k_{row}**max**	1	1	0.8	1	1	1	1	1	1
k_{row}**crit**	0.883	0.703	0.530	0.621	0.772	0.462	0.402	0.565	0.841
S_{wr}	0.240	0.176	0.310	0.201	0.334	0.439	0.375	0.453	0.371
S_{or}	0.203	0.221	0.270	0.169	0.241	0.270	0.260	0.338	0.274
S_{wr}**@**k_{row}**crit**	0.270	0.205	0.400	0.264	0.377	0.468	0.412	0.474	0.477
S_w**max**	0.797	0.779	0.730	0.831	0.759	0.730	0.740	0.662	0.726

Table 9. Gas/oil relative permeability critical points derived from laboratory data.

	Sample 3-7	*UNOCAL**	*Core 19@3000 psi*	*Core 19@3600 psi*	*Core 19@4000 psi*	*Core L5@3000 psi*	*Core L5@3500 psi*	*Core L5@4000 psi*
k_{rg}**max**	0.076	0.950	0.058	0.145	0.141	0.045	0.175	0.142
k_{rog}**max**	1	0.8	1	1	1	1	1	1

k_{rog}crit	0.380	0.730	0.669	0.923	0.326	0.753	0.813	0.885
S_{gr}	0.102	0.020	0.193	0.154	0.127	0.094	0.183	0.132
S_{lr}	0.393	0.310	0.164	0.156	0.140	0.231	0.221	0.175
S_{gr}@k_{rog}crit	0.102	0.020	0.257	0.223	0.200	0.162	0.243	0.202
$S_g$max	0.607	0.690	0.836	0.844	0.860	0.769	0.779	0.825

7.4 FITTING MICP DATA USING LABORATORY DATA ENDPOINTS AND 'B' AND 'C' EXPONENTS

To understand how well the method to create two- and three-phase relative permeability curves from capillary pressure data performs, a number of laboratory data containing both relative permeability and capillary pressure from Farnsworth core and the literature were studied, described above. The goal was to elucidate any common fitting parameters that could be applied to capillary pressure data that lack corresponding relative permeability data. Below I discuss the results of fitting the capillary pressure exponent *b* and effective saturation exponent *c* for Equation 3 and Equation 4 to the laboratory data.

7.4.1 Two-phase data fitting

I applied the critical end-points described in 7.5 to Equation 3 and Equation 4 and adjusted the *b* and *c* exponents to fit the relative permeability curves to the laboratory-measured data. I used the least-squares regression analysis to minimize the misfit between the laboratory data and calculated data for the wetting (k_{rw}) and non-wetting phases (k_{rn}) curves (Table 10). I determined that for the non-wetting phase (k_{rn}) a *b* exponent of **0.5** was the best fit, and for the wetting phase (k_{rw}) a *b* exponent of **-1** gave the best fit (Table 11). See 11.1 in Appendix I for more details on the goodness of fit analysis with R^2 values.

Applying a wetting phase *b* value of -1 simplifies Equation 3, removing the capillary pressure term and making the wetting phase relative permeability a saturation relationship only, shown in Equation 10. This is similar to Corey's wetting phase relative permeability empirical formula (Corey, 1954). When the non-wetting phase *b* value of 0.5 is substituted into Equation 4, it simplifies to saturation over capillary pressure cubed relationship (Equation 11).

Equation 10

$$k_{rw} = k_{w\,max} * \left(\frac{S_w - S_{wr}}{S_w^{max} - S_{wr}}\right)^c * \frac{(S_{wr} + S_w)}{(S_{wr} + S_w^{max})}$$

Equation 11

$$k_{rn} = k_{n\,max} * \left(\frac{S_w^{max} - S_w}{S_w^{max} - S_{wr}}\right)^c * \frac{\left(\frac{S_w}{Pc(S_w)^3} + \frac{S_w^{max}}{Pc(S_w^{max})^3}\right)}{\left(\frac{S_{wr}}{Pc(S_{wr})^3} + \frac{S_w^{max}}{Pc(S_w^{max})^3}\right)}$$

The effective saturation exponent '*c*' is unique for each sample analyzed. There does seem to be an inverse relationship between the wetting and non-wetting phase data. As one exponent gets larger, the other gets smaller, but there is no correlation between lithologies. The average of all of the samples was

3.03 for the wetting phase and 3.60 for the non-wetting phase (Table 11). Unlike the capillary pressure exponent, the effective saturation exponent cannot be used to simplify the Equation 3 or Equation 4.

Table 10 Least-squares analysis of the goodness of fit between the curves generated by the Pc-to-RP method and the laboratory data.

Least Squares Data Analysis		
	Wetting (k_{rw})	***Non-Wetting (k_{rn})***
Basal Cambrian Sandstone	6.69E-04	1.17E-03
Wabamun - low perm	9.15E-04	8.60E-04
Ellerslie Sandstone	3.75E-04	6.41E-05
Viking Sandstone	7.04E-05	3.29E-05
Cooking Lake Carbonate	1.35E-04	7.55E-05
Nisku Carbonate	2.94E-04	2.82E-05
Berea Sandstone	2.98E-02	1.98E-04
Mt Simon Sandstone	1.24E-02	3.50E-04
Paaratte Sandstone	6.08E-02	7.83E-04
Tuscaloosa Sandstone	2.29E-03	4.06E-05

Table 11. Fitting parameters for the capillary pressure exponent 'b' and the effective saturation exponent 'c' derived from fitting the curves to the laboratory data using the sum of least squares minimization algorithm. This data is for the two-phase gas/water system using the laboratory relative permeability and capillary pressure data taken from the literature (B. Bennion & Bachu, 2005, 2006; S. C. M. Krevor, et al., 2012).

Formation Name	*Capillary Pressure exponent 'b'*		*Effective Saturation exponent 'c'*	
	b-k_{rn}	*b-k_{rw}*	*c-k_{rn}*	*c-k_{rw}*
Basal Cambrian Sandstone	0.5	-1	5.23	1.34
Wabamun - low perm	0.5	-1	5.99	1.22
Ellerslie Sandstone	0.5	-1	2.18	1.89
Viking Sandston	0.5	-1	2.93	2.93
Cooking Lake Carbonate	0.5	-1	4.55	3.01
Nisku Carbonate	0.5	-1	1.11	2.32
Berea Sandstone	0.5	-1	3.05	3.29
Mt Simon Sandstone	0.5	-1	1.80	5.76
Paaratte Sandstone	0.5	-1	3.52	6.10
Tuscaloosa Sandstone	0.5	-1	5.66	2.50
Likely Fitting Parameters	*0.5*	*-1*	*3.60*	*3.03*

7.4.2 Three-Phase Data Fitting

Following the same workflow I used for the two-phase data fitting, I applied the critical end-points described in 7.5 *Note on Critical End-Point Modification* to Equation 3 and Equation 4 and adjusted the *b* and *c* exponents to fit the relative permeability curves to the laboratory-measured data. I again use least-squares regression analysis to minimize the misfit between the laboratory data and calculated data for the

wetting (k_{rw}) and non-wetting phases (k_{row}) curves for the oil/water fluid pair and the wetting (k_{rog}) and non-wetting (k_{rg}) curves for the gas/oil fluid pair (Table 12). Here the fit is not as good as the two-phase system, with the gas/oil pair having a worse fit than the oil/water pair. I believe that the fit is still acceptable for determining the capillary pressure exponent *b* and the effective saturation exponent *c*.

Table 12 Final sum of least squares values for each of the four curves in the three-phase relative permeability relationship.

Sum of Squares Minimization				
	Gas	*Oil*	*Oil*	*Water*
PU-1	1.49E-03	2.66E-02	2.75E-02	4.95E-03
PU-2	8.71E-04	2.70E-02	9.70E-02	2.15E-03
LR-19	2.06E-02	3.14E-01	3.81E-02	3.22E-03
LR-L5	6.92E-03	6.37E-01	2.82E-02	4.53E-03

For the oil/water fluid pair, the capillary pressure exponent *b* for the wetting phase (k_{rw}) is likely -0.5, and for the non-wetting phase (k_{row}) 0.1 (Table 13). The effective saturation exponent *c* for the wetting phase (k_{rw}) is likely 1.0 and for the non-wetting phase (k_{row}) 2.8 (Table 13). There is variability around these values, and more data would be needed to refine these points as four sample points are not enough to gain good statistical insight.

Table 13 Fitting parameters for the capillary pressure exponent 'b' and the effective saturation exponent 'c' for the oil/water fluid pair.

Sample ID	*Capillary Pressure exponent 'b' (oil/water)*		*Effective Saturation exponent 'c' (oil/water)*	
	b-k_{rw}	*b-k_{row}*	*c-k_{rw}*	*c-k_{row}*
PU 1 sample 5-1	-0.5	0.84	1	2.80
PU 2 Sample 3-9	-0.5	0.11	0.1	2.86
NMT1 Core19	-1	-0.5	1.18	3.66
NMT2 CoreL5	-0.5	0.1	1	2.82
Likely fitting parameters	-0.5	0.1	1	2.8

Similar variability is also seen during the gas/oil fluid pair parameter fitting. The capillary pressure exponent 'b' is relatively consistent at -0.5 for the wetting phase (k_{rog}) and 0.5 for the non-wetting phase (k_{rg}) (Table 14). The effective saturation exponent 'c' looks to be correlated to who did the testing for both the non-wetting phase. The samples from CUPB have a '*c*' exponent for the non-wetting phase (k_{rg}) of 3.47-3.95, while Rasmussen et al. (2019) have values of 9 to 9.65 (Table 14).

Table 14 Fitting parameters for the capillary pressure exponent 'b' and the effective saturation exponent 'c' for the gas/oil fluid pair.

Sample ID	*Capillary Pressure exponent 'b' (gas/oil)*		*Effective Saturation exponent 'c' (gas/oil)*	
	b-k_{rg}	*b-k_{rog}*	*c-k_{rg}*	*c-k_{rog}*
PU 1 Sample 3-7	0.87	-0.5	3.95	1.14

PU 2 Sample 3-7	0.58	-0.5	3.47	1.24
NMT1 Core19	0.5	-0.5	9	2
NMT2 CoreL5	0.20	-2	9.65	0.85
Likely fitting parameters	0.5	-0.5	3.5 or 9	1

By applying the 'likely fitting parameters' from Table 13 and Table 14 to Equation 3 and Equation 4, I derive the following four equations that describe the oil/water and gas/oil fluid pairs needed to describe a three-phase relationship. For the oil/water fluid pair, the wetting phase relative permeability (k_{rw}) Equation 3 simplifies to Equation 12, and for the non-wetting phase relative permeability (k_{row}) Equation 4 simplifies to Equation 13. For the gas/oil fluid pair, the wetting phase relative permeability (k_{rog}) Equation 3 simplifies to Equation 14, which has the same saturation/capillary pressure relationship as the wetting phase relative permeability for the oil/water fluid pair. The gas/oil non-wetting phase relative permeability (k_{rg}) Equation 4 simplifies to Equation 15, a saturation/cubic capillary pressure relationship. See 11.2 in Appendix I for more details on the data fitting and R^2 values.

Equation 12

$$k_{rw} = k_{w\,max} * \left(\frac{S_w - S_{wr}}{S_w^{max} - S_{wr}}\right) * \frac{\left(\frac{S_{wr}}{Pc(S_{wr})} + \frac{S_w}{Pc(S_w)}\right)}{\left(\frac{S_{wr}}{Pc(S_{wr})} + \frac{S_w^{max}}{Pc(S_w^{max})}\right)}$$

Equation 13

$$k_{row} = k_{ow\,max} * \left(\frac{S_w^{max} - S_w}{S_w^{max} - S_{wr}}\right)^{2.8} * \frac{\left(\frac{S_w}{Pc(S_w)^{2.2}} + \frac{S_w^{max}}{Pc(S_w^{max})^{2.2}}\right)}{\left(\frac{S_{wr}}{Pc(S_{wr})^{2.2}} + \frac{S_w^{max}}{Pc(S_w^{max})^{2.2}}\right)}$$

Equation 14

$$k_{rog} = k_{og\,max} * \left(\frac{S_l - S_{lr}}{S_l^{max} - S_{lr}}\right) * \frac{\left(\frac{S_{lr}}{Pc(S_l)} + \frac{S_l}{Pc(S_l^{max})}\right)}{\left(\frac{S_{lr}}{Pc(S_{lr})} + \frac{S_l^{max}}{Pc(S_l^{max})}\right)}$$

Equation 15

$$k_{rg} = k_{g\,max} * \left(\frac{S_l^{max} - S_l}{S_l^{max} - S_{lr}}\right)^{3.5} * \frac{\left(\frac{S_l}{Pc(S_l)^3} + \frac{S_l^{max}}{Pc(S_l^{max})^3}\right)}{\left(\frac{S_{lr}}{Pc(S_{lr})^3} + \frac{S_l^{max}}{Pc(S_l^{max})^3}\right)}$$

7.5 NOTE ON CRITICAL END-POINT MODIFICATION

Fitting this method to laboratory relative permeability data collected by Lindsay Rasmussen and China Petroleum University Beijing indicated how much the saturation and relative permeability endpoints

needed to be modified to get the predicted curves to line up with the laboratory data. Modifiers were derived by tabulating the maximum phase relative permeability, the maximum and minimum water saturation, and the maximum and minimum gas saturation from the curves fitted to the laboratory data. I then used the averaged these data points to determine the modifier for each critical end-point (see Table 15). These modifiers were then used to adjust the critical end-points of the curves created using the Pc-to-RP method, bringing the calculated curves more in-line with the laboratory data. This work created two suites of relative permeability curves from the corresponding MICP data, one suite that is '*fit*' using these critical end-point modifiers and one suite that is '*raw*,' using only the method to determine the critical end-points with no modifications applied.

It is important to note that the total liquid saturation, used for calculating the gas/oil fluid pair relative permeability, is the oil saturation plus residual water saturation ($S_l=S_{wr}+S_o$). This is done to conform to formatting requirements for the gas/oil relative permeability table in the Eclipse© numerical simulator.

Table 15. Critical end-point modification percentages as determined from fitting the curves generated by the Pc-to-RP method to laboratory-measured relative permeability and capillary pressure data.

Critical Point Modification			
Oil/Water		*Gas/Oil*	
$k_{rw\text{-}max}$	-70.0%	$k_{rg\text{-}max}$	-80.0%
$k_{row\text{-}max}$	5.0%	$k_{rog\text{-}max}$	5.0%
S_{wr}	0.0%	S_{lr}	$S_{wr}+(1-S_{w\text{-}max})$
$S_{w\text{-}max}$	-5.0%	$S_{l\text{-}max}$	$S_{w\text{-}max}$

7.6 NOTE ON TORTUOSITY

Tortuosity, as defined in (9) of the Pc-to-RP method described in section 6.3 *Theory and Derivation*, is the fluid path length (l) over the sample length (L). The tortuosity was not measured or reported for the three-phase samples from Farnsworth or the two-phase samples from the literature. For this study, I had to estimate a tortuosity value to calculate the permeability from the capillary pressure data using Equation 1 (Purcell, 1949). The MICP data had a calculated permeability value from the original testing. The tortuosity value was used to 'tune' the max oil/water permeability value I calculated using the Pc-to-RP method to the value calculated by the laboratory value. The testing lab used the Swanson method (Equation 5 and Equation 6) to calculate the permeability from the MICP data (Swanson, 1981). This method doesn't use tortuosity to calculate the permeability but a constant and exponent that are related to the sample's lithology, just like the tortuosity. Uncertainty in these numbers can cause the calculated permeability using Equation 1 to be different from Equation 5 and Equation 6. So, by tuning tortuosity, I was able to match the permeability between the two methods, in essence calibrating the maximum calculated permeability to the lab data.

7.7 NOTE ON EFFECTS OF WETTABILITY ON THE PC-TO-RP METHOD

The wettability of the system does not affect the relative permeability curves as calculated by Equation 3 and Equation 4. The curve will be the same for a water-wet, mixed-wet, or oil-wet system. The system's wettability does affect the capillary pressure curve. The magnitude of the capillary pressure scales with the magnitude of the system's wettability, going from large positive capillary pressure for a strongly water-wet system to large negative capillary pressure for a strongly oil-wet system. As the system approaches a mixed-wet state, the capillary pressure reduces to zero as you approach a contact angle of

90° (Equation 9). The calculated permeability (k) and effective permeability (k_e) end-points are also affected by the system's wettability. Still, they scale proportionally to the wettability making the calculated relative permeability end-points insensitive to wettability. The insensitivity to wettability shows that this method can, in theory, calculate the rock's intrinsic relative permeability.

8 RESULTS OF THE PC-TO-RP METHOD

A suite of 16 three-phase relative permeability and capillary pressure relationships are created using the Pc-to-RP method described in Section 6 *Theory and Method Development* and the Farnsworth Unit's data described in Section 7. Figure 2 thru Figure 17 show the gas/oil relative permeability in (a) and the oil/water relative permeability in (b) for curves fitted to the critical end-points in Table 15 (fit) and for curves where the critical end-points are determined by the method alone (raw). The mercury intrusion capillary pressure (MICP) data is plotted in (c), and the calculated reservoir capillary pressure is shown in (d) under water-wet (blue line), mixed-wet (red line), and oil-wet (green line) fluid conditions.

This method creates relative permeability curves that are dictated by the strength and shape of the capillary pressure data. Using only MICP data paired with the assumed wettability conditions of the reservoir, an accurate relative permeability relationship can be derived for the formation of interest. Adding critical end-points derived from laboratory-measured relative permeability data for the reservoir of interest can increase the fit of the resulting curves, but special attention must be given to the maximum relative permeability. This value comes from calculating the maximum permeability and the effective permeability over a specified saturation range. Assuming the wetting phase effective permeability is at the maximum wetting phase saturation consistently gives results similar to the laboratory data and is likely an appropriate place to determine this value. Assuming the non-wetting phase effective permeability is at the angle of 45° on the capillary pressure curve is probably not a correct assumption. Results show a poor fit to the laboratory data when that point is used. Other options need to be investigated to determine a better method of estimating non-wetting phase effective permeability.

A consistent result of this method is that the 'raw' k_{rg} and k_{rw} curves span a much wider range of relative permeability and saturation values than the corresponding 'fit' curves. This is a result of applying the modifiers from Table 15. The laboratory relative permeability data indicates a lower gas (CO_2) and water maximum relative permeabilities than predicted from just the MICP data. The higher pressure range over which the MICP tests are performed compared to the stable pressure of a relative permeability test could be the cause of this difference between laboratory and calculated curves. The higher range of pressures in a MICP test may capture more of the dynamic flow processes across the range of pore sizes, similar to what happens at reservoir conditions. This may be why the relative permeability curve derived from the MICP data span a higher saturation and relative permeability range.

Using the maximum relative permeability modifiers (Table 15) does not account for up-scaling from the laboratory to the reservoir scale. The UNOCAL three-phase relationship (Appendix I Figure 28) indicates a much higher maximum k_{rg} than any of the SWP laboratory data (Rasmussen, et al., 2019; Wang, 2017). According to May (1987), these curves were 'modified for simulation' from the laboratory data. The non-upscaled data is not provided for comparison, unfortunately. Based on the laboratory data from the SWP, I would assume the authors fit the lab data to an empirical relationship that extrapolated the k_{rg} leg to a relative permeability of 1.0. The 'raw' curves appear to fit the UNOCAL curves better than the 'fit' curves. The Pc-toRP method may provide a way to develop relative permeability relationships that are 'up-scaled' from the laboratory data by not applying any modifiers. More relative permeability laboratory testing would need to be done to elucidate better fitting parameters and modifiers for the Morrow 'B' Sandstone.

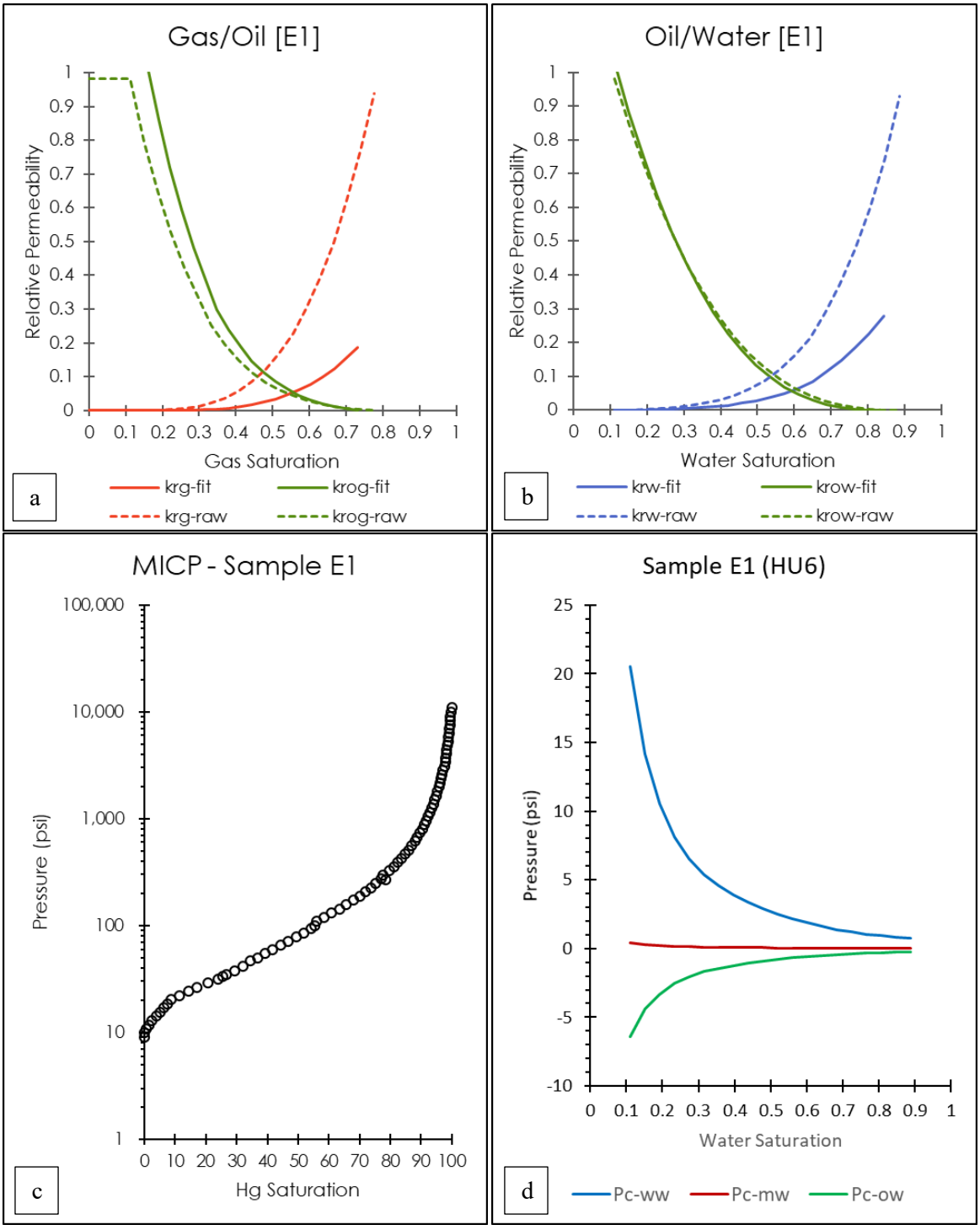

Figure 2 Results of the Pc-to-RP method applied to Sample E1(HU6), (a) is the gas/oil relative permeability curves (fit and raw), (b) is the oil/water relative permeability curves (fit and raw), (c) is the MICP data, and (d) are the water-wet (ww), mixed-wet (mw), and oil-wet (ow) capillary pressure curves.

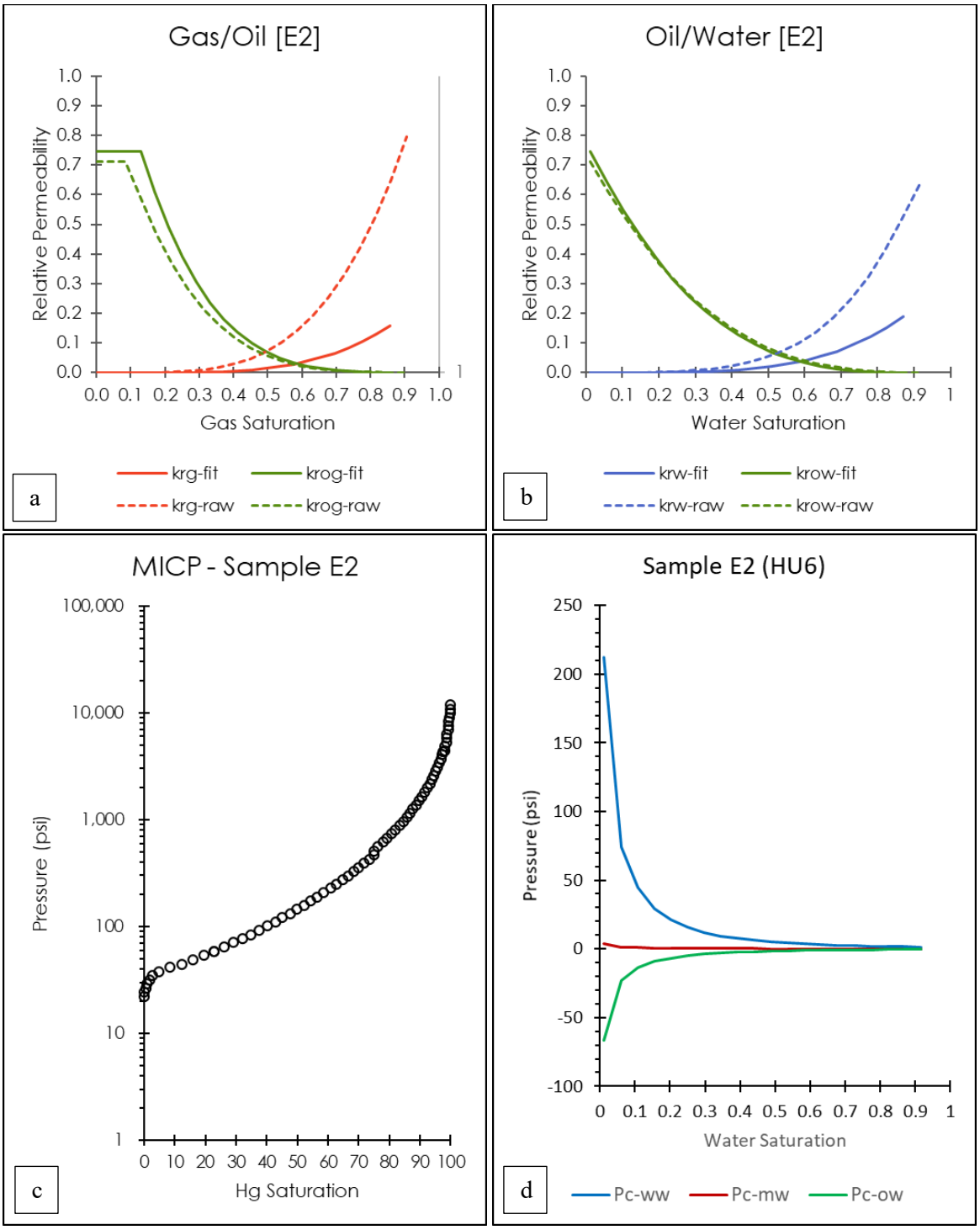

Figure 3 Results of the Pc-to-RP method applied to Sample E2 (HU6), (a) is the gas/oil relative permeability curves (fit and raw), (b) is the oil/water relative permeability curves (fit and raw), (c) is the MICP data, and (d) are the water-wet (ww), mixed-wet (mw), and oil-wet (ow) capillary pressure curves.

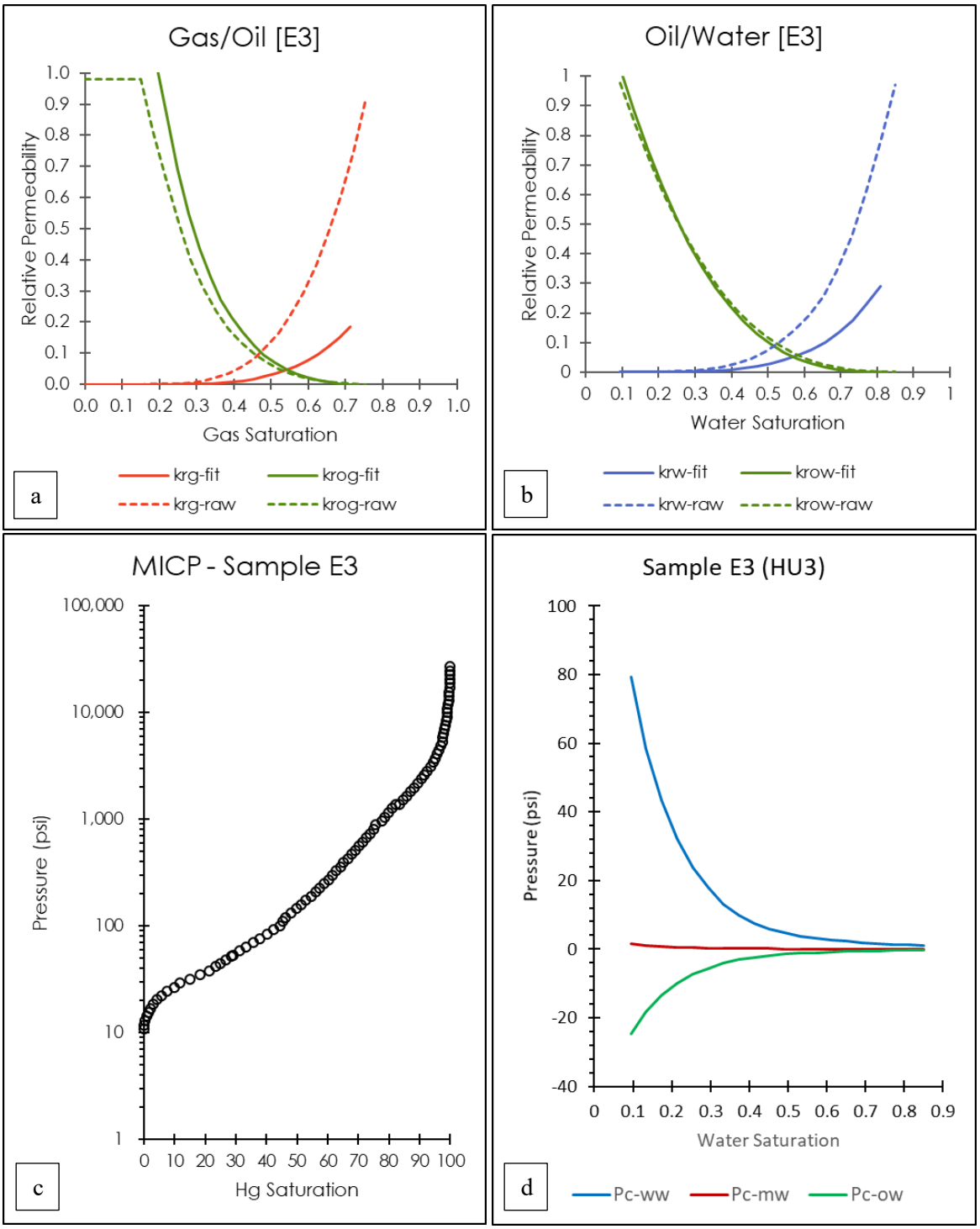

Figure 4 Results of the Pc-to-RP method applied to Sample E3 (HU3), (a) is the gas/oil relative permeability curves (fit and raw), (b) is the oil/water relative permeability curves (fit and raw), (c) is the MICP data, and (d) are the water-wet (ww), mixed-wet (mw), and oil-wet (ow) capillary pressure curves.

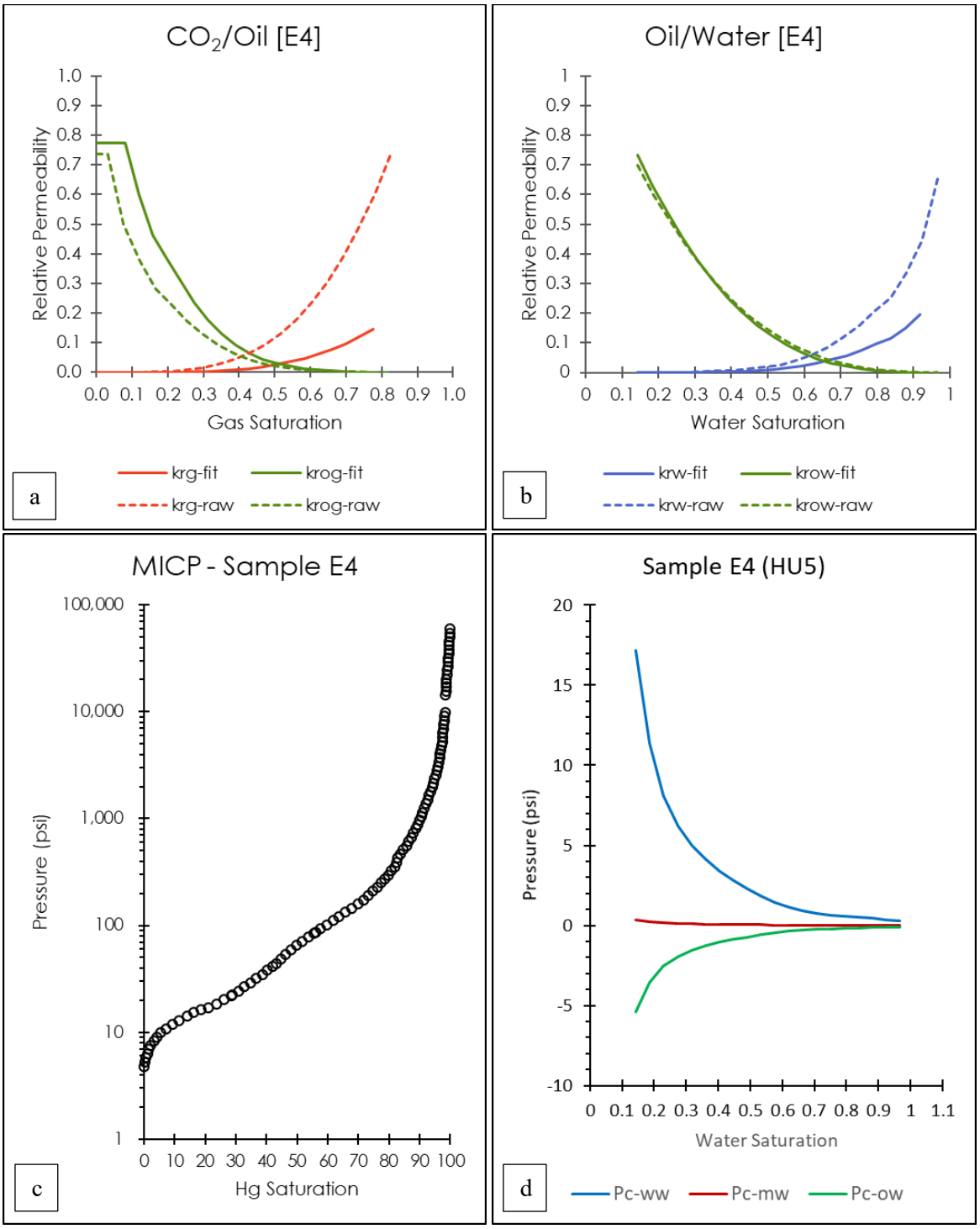

Figure 5 Results of the Pc-to-RP method applied to Sample E4 (HU5), (a) is the gas/oil relative permeability curves (fit and raw), (b) is the oil/water relative permeability curves (fit and raw), (c) is the MICP data, and (d) are the water-wet (ww), mixed-wet (mw), and oil-wet (ow) capillary pressure curves.

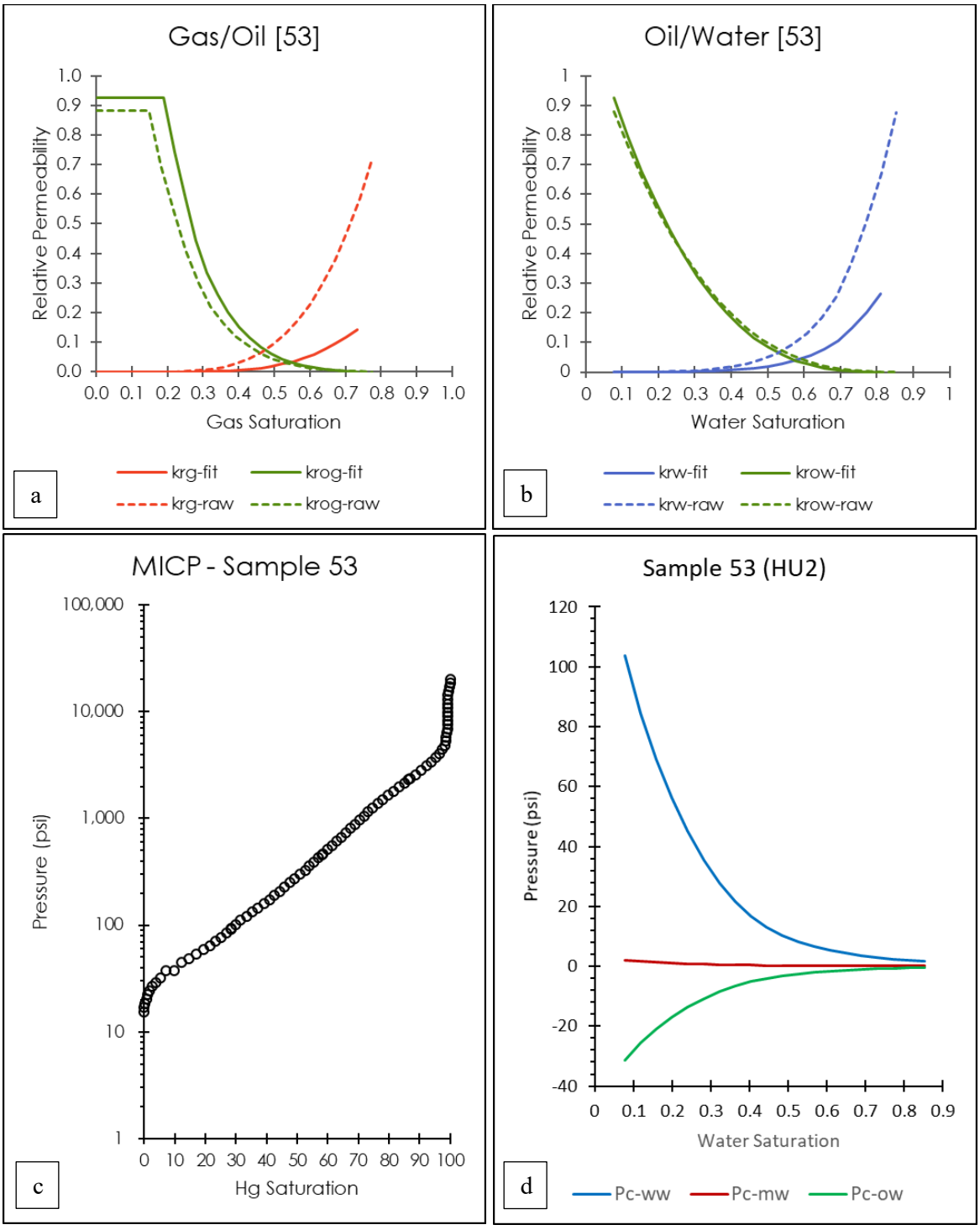

Figure 6 Results of the Pc-to-RP method applied to Sample 53 (HU2), (a) is the gas/oil relative permeability curves (fit and raw), (b) is the oil/water relative permeability curves (fit and raw), (c) is the MICP data, and (d) are the water-wet (ww), mixed-wet (mw), and oil-wet (ow) capillary pressure curves.

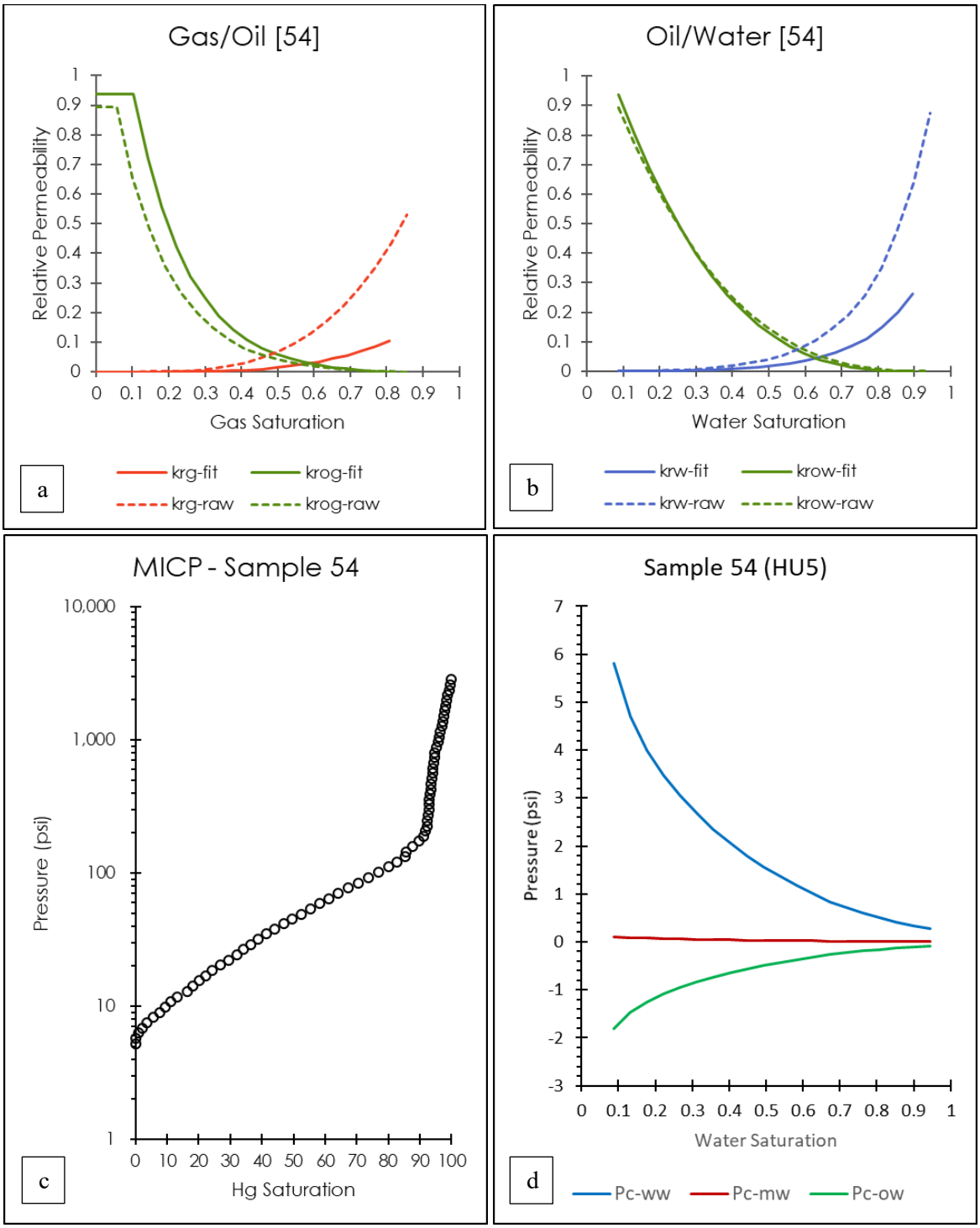

Figure 7 Results of the Pc-to-RP method applied to Sample 54 (HU5), (a) is the gas/oil relative permeability curves (fit and raw), (b) is the oil/water relative permeability curves (fit and raw), (c) is the MICP data, and (d) are the water-wet (ww), mixed-wet (mw), and oil-wet (ow) capillary pressure curves.

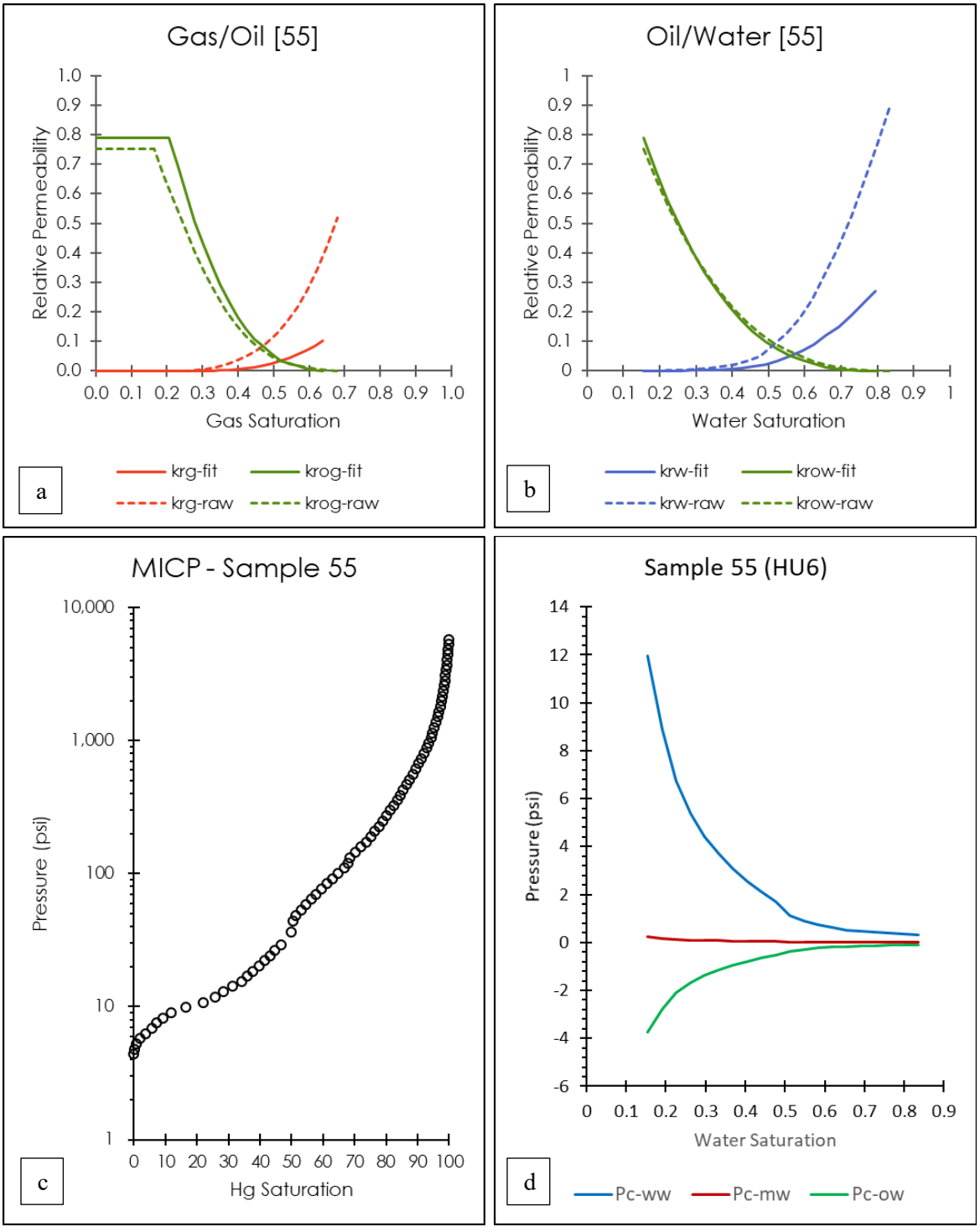

Figure 8 Results of the Pc-to-RP method applied to Sample 55 (HU5), (a) is the gas/oil relative permeability curves (fit and raw), (b) is the oil/water relative permeability curves (fit and raw), (c) is the MICP data, and (d) are the water-wet (ww), mixed-wet (mw), and oil-wet (ow) capillary pressure curves.

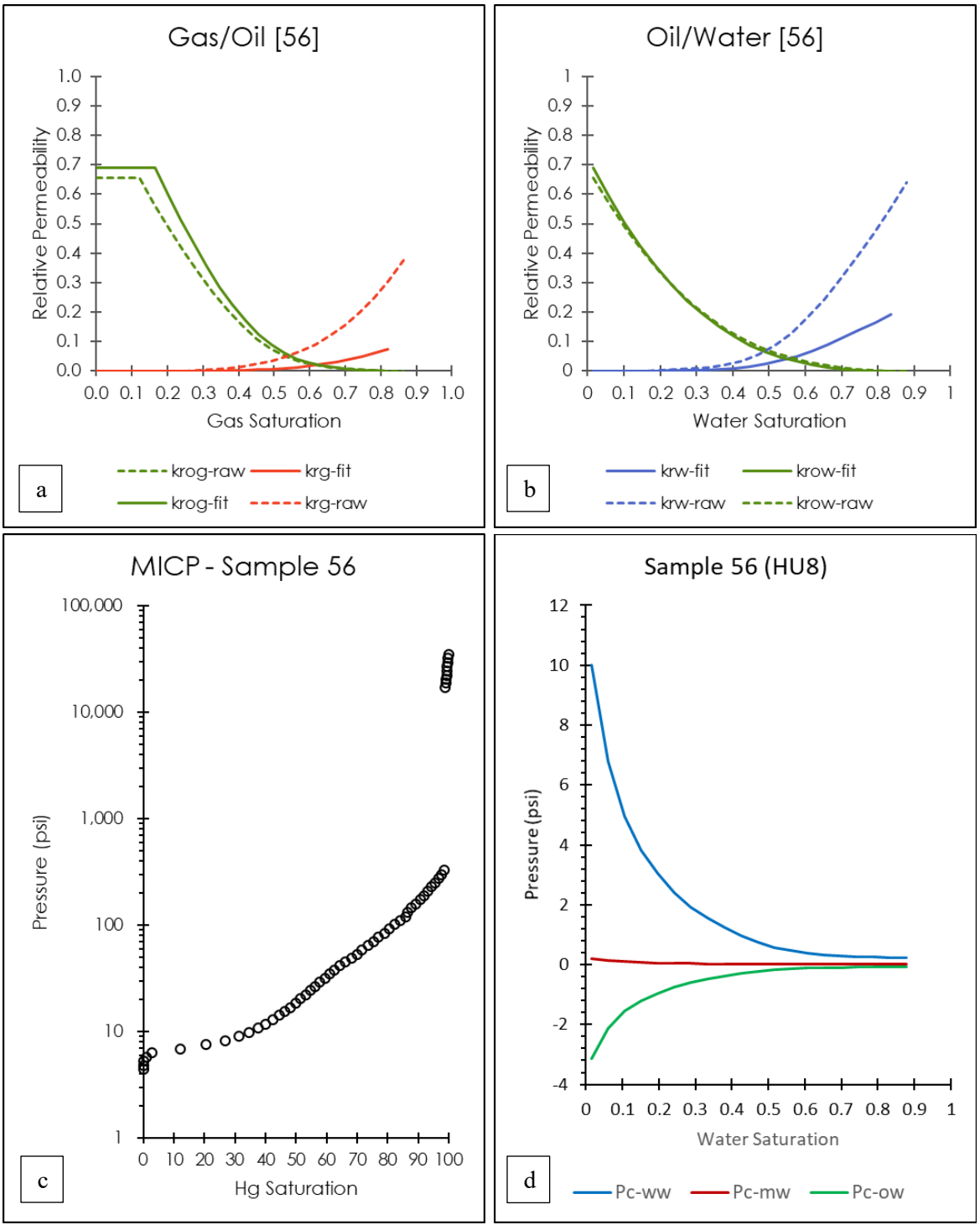

Figure 9 Results of the Pc-to-RP method applied to Sample 56 (HU8), (a) is the gas/oil relative permeability curves (fit and raw), (b) is the oil/water relative permeability curves (fit and raw), (c) is the MICP data, and (d) are the water-wet (ww), mixed-wet (mw), and oil-wet (ow) capillary pressure curves.

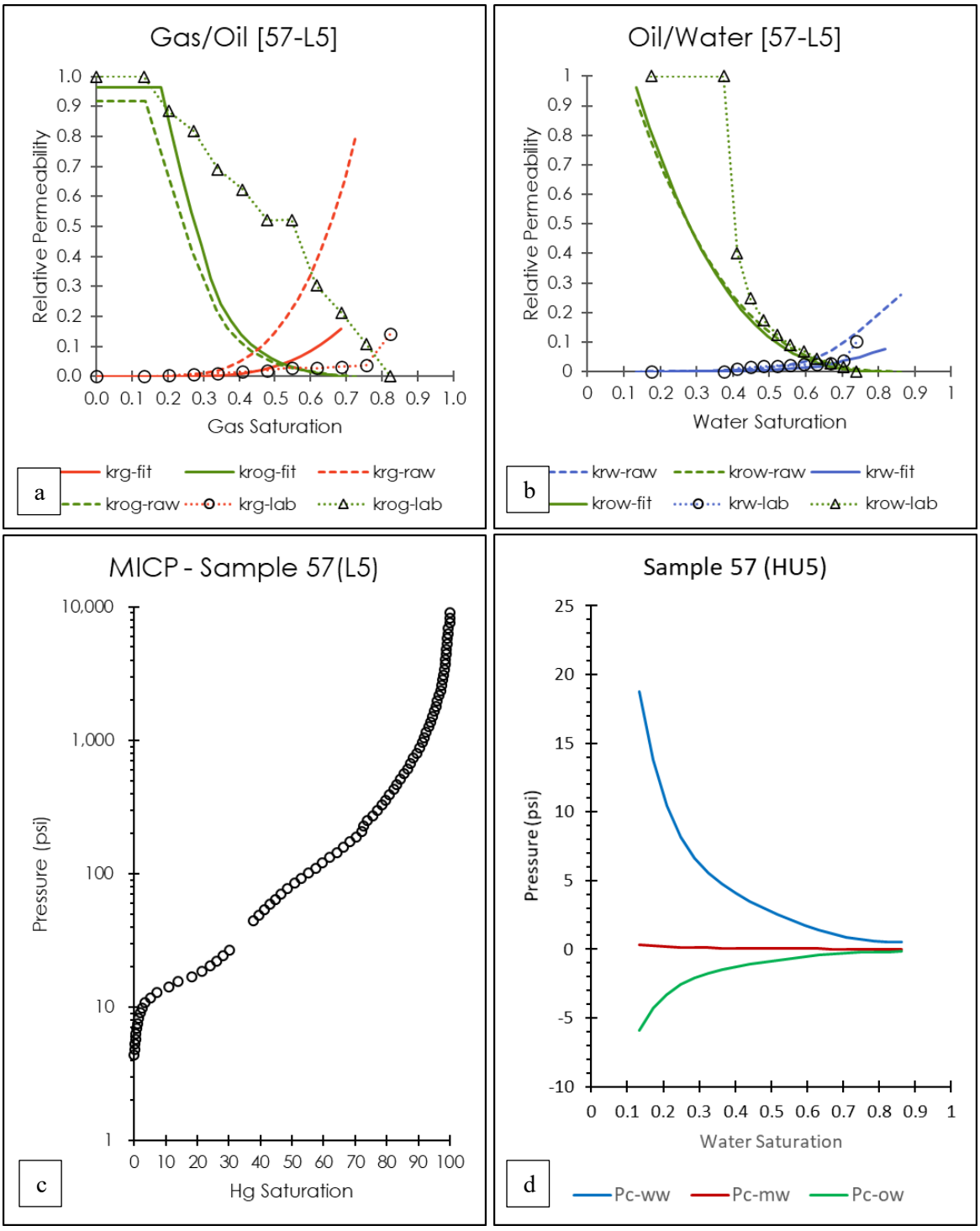

Figure 10 Results of the Pc-to-RP method applied to Sample 57 (HU5), (a) is the gas/oil relative permeability curves (fit and raw), (b) is the oil/water relative permeability curves (fit and raw), (c) is the MICP data, and (d) are the water-wet (ww), mixed-wet (mw), and oil-wet (ow) capillary pressure curves. The lab relative permeability curves were measured on sample L5 by Rasmussen et al. (2019).

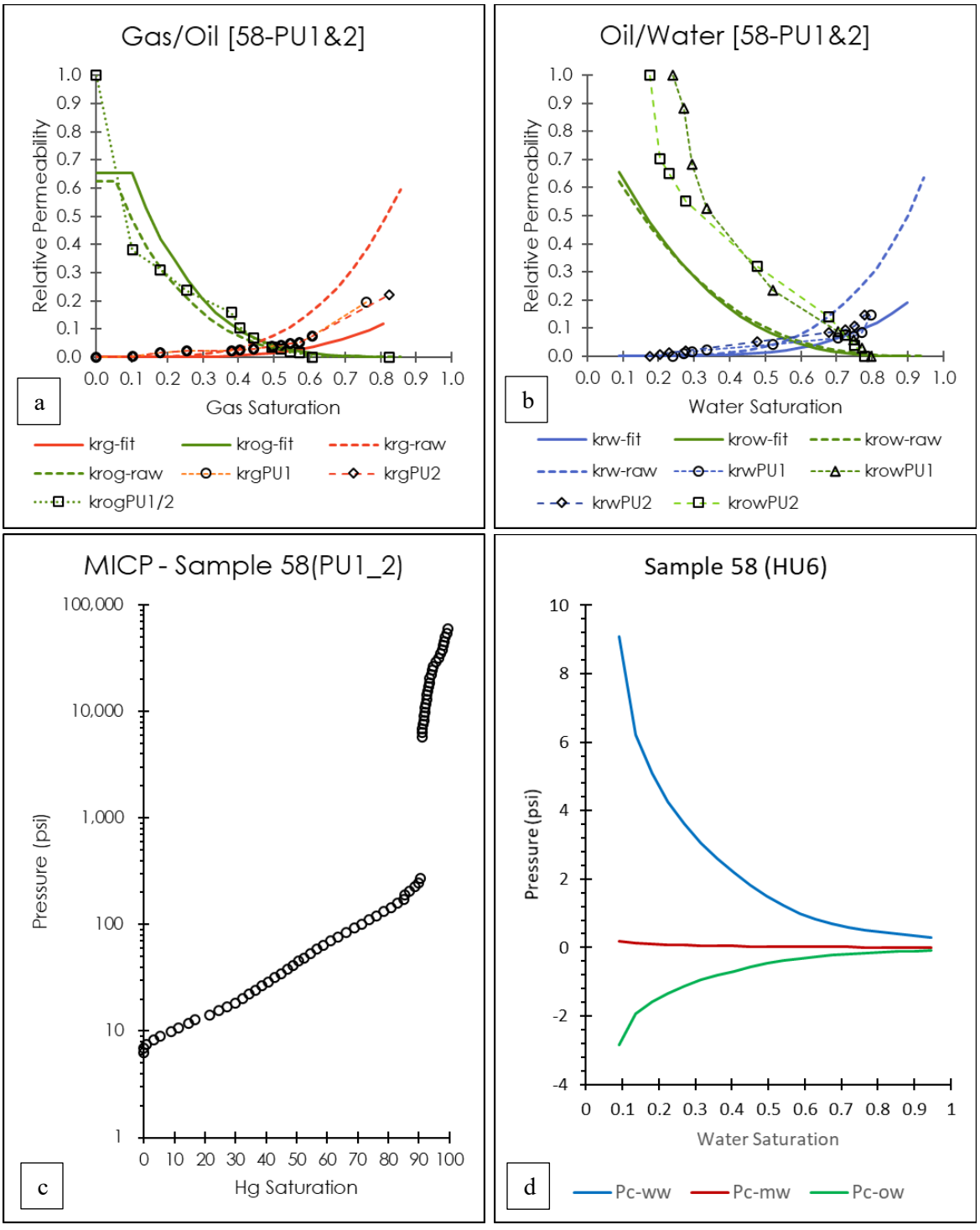

Figure 11 Results of the Pc-to-RP method applied to Sample 58 (HU6), (a) is the gas/oil relative permeability curves (fit and raw) and the laboratory measured data in open symbols, (b) is the oil/water relative permeability curves (fit and raw), (c) is the MICP data, and (d) are the water-wet (ww), mixed-wet (mw), and oil-wet (ow) capillary pressure curves. The lab relative permeability curves were measured on sample 58 by Wang (2017).

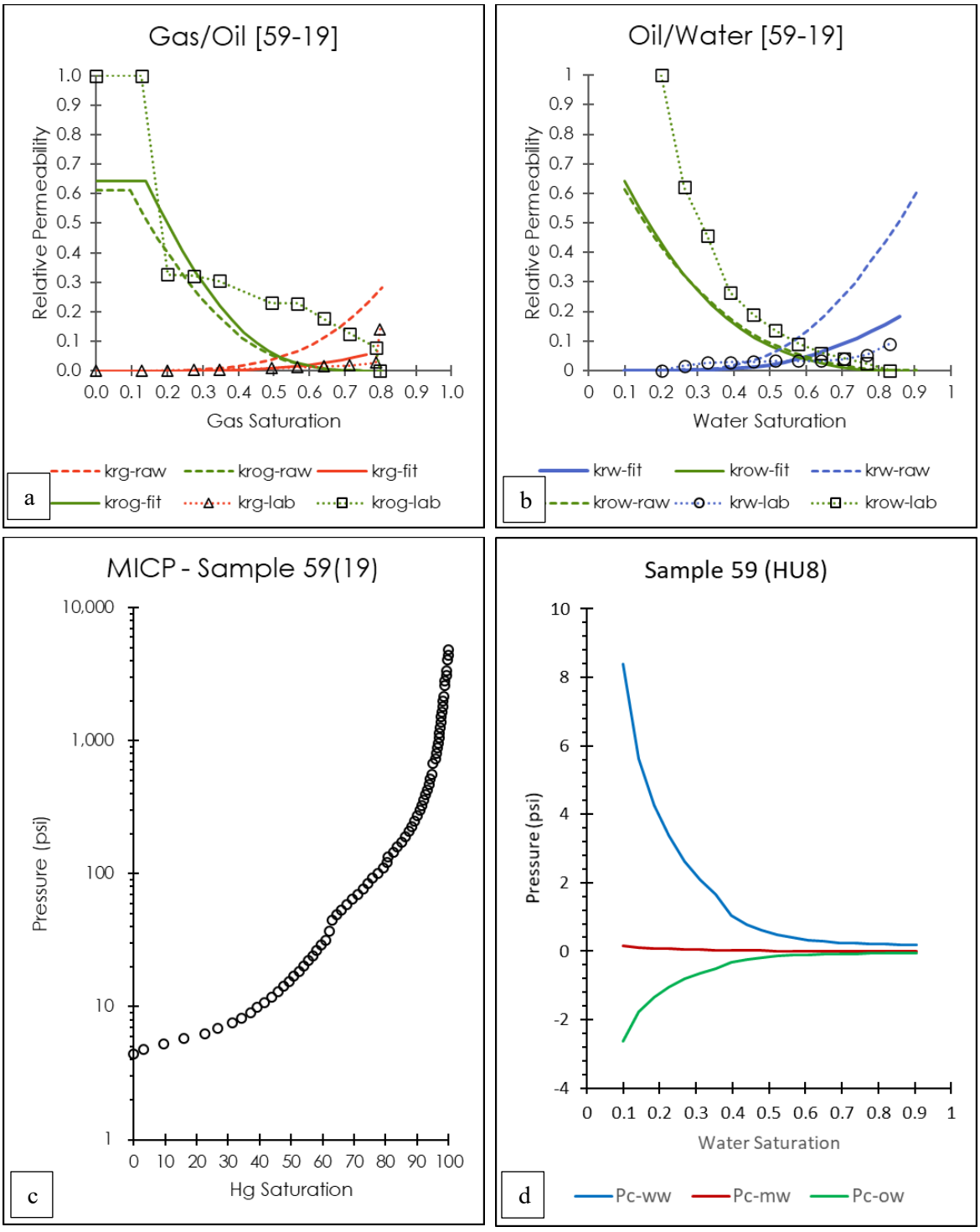

Figure 12 Results of the Pc-to-RP method applied to Sample 59 (HU8), (a) is the gas/oil relative permeability curves (fit and raw) and the laboratory measured data in open symbols, (b) is the oil/water relative permeability curves (fit and raw), (c) is the MICP data, and (d) are the water-wet (ww), mixed-wet (mw), and oil-wet (ow) capillary pressure curves. The lab relative permeability curves were measured on sample 19 by Rasmussen et al. (2019).

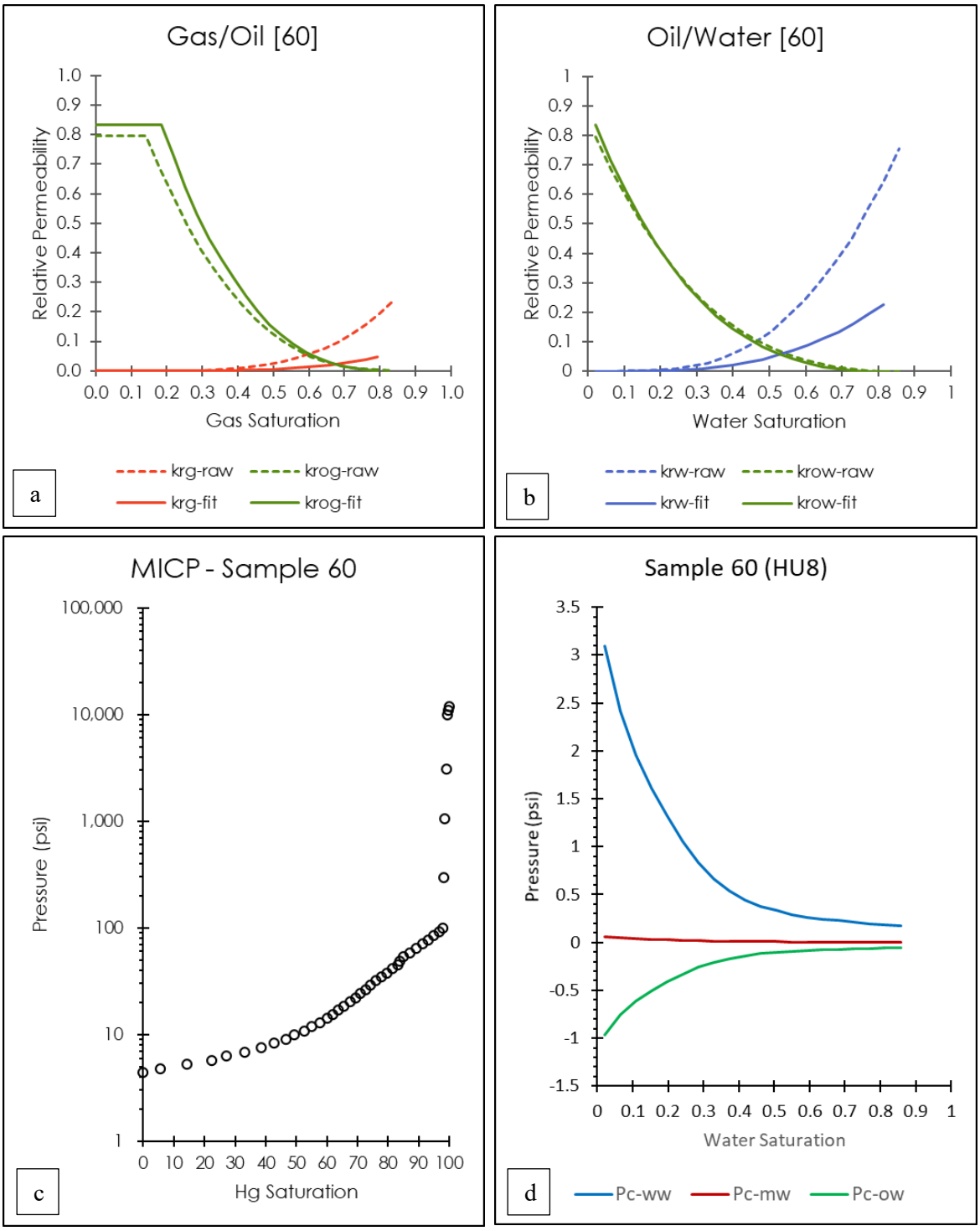

Figure 13 Results of the Pc-to-RP method applied to Sample 60 (HU8), (a) is the gas/oil relative permeability curves (fit and raw), (b) is the oil/water relative permeability curves (fit and raw), (c) is the MICP data, and (d) are the water-wet (ww), mixed-wet (mw), and oil-wet (ow) capillary pressure curves.

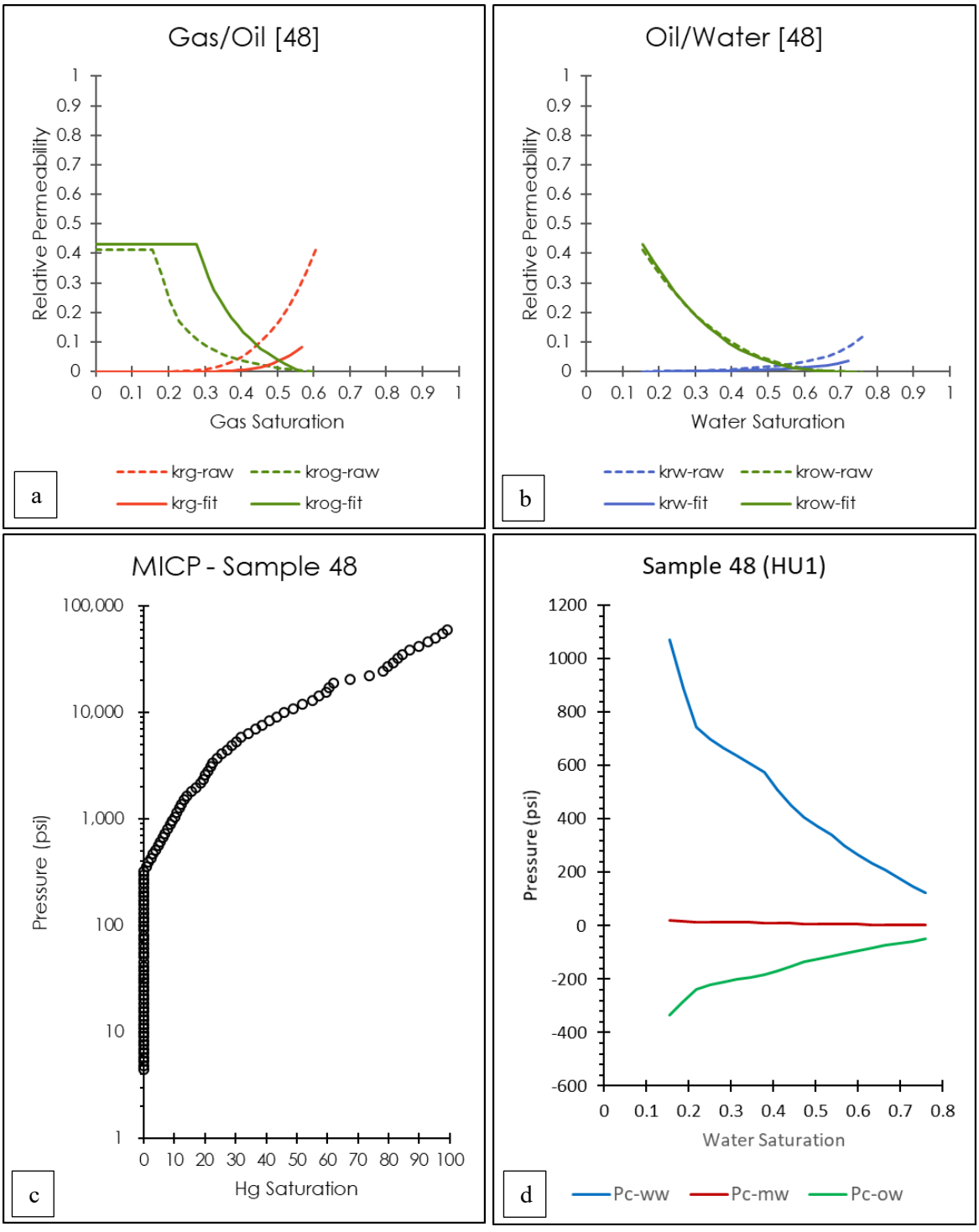

Figure 14 Results of the Pc-to-RP method applied to Sample 48 (HU1), (a) is the gas/oil relative permeability curves (fit and raw), (b) is the oil/water relative permeability curves (fit and raw), (c) is the MICP data, and (d) are the water-wet (ww), mixed-wet (mw), and oil-wet (ow) capillary pressure curves.

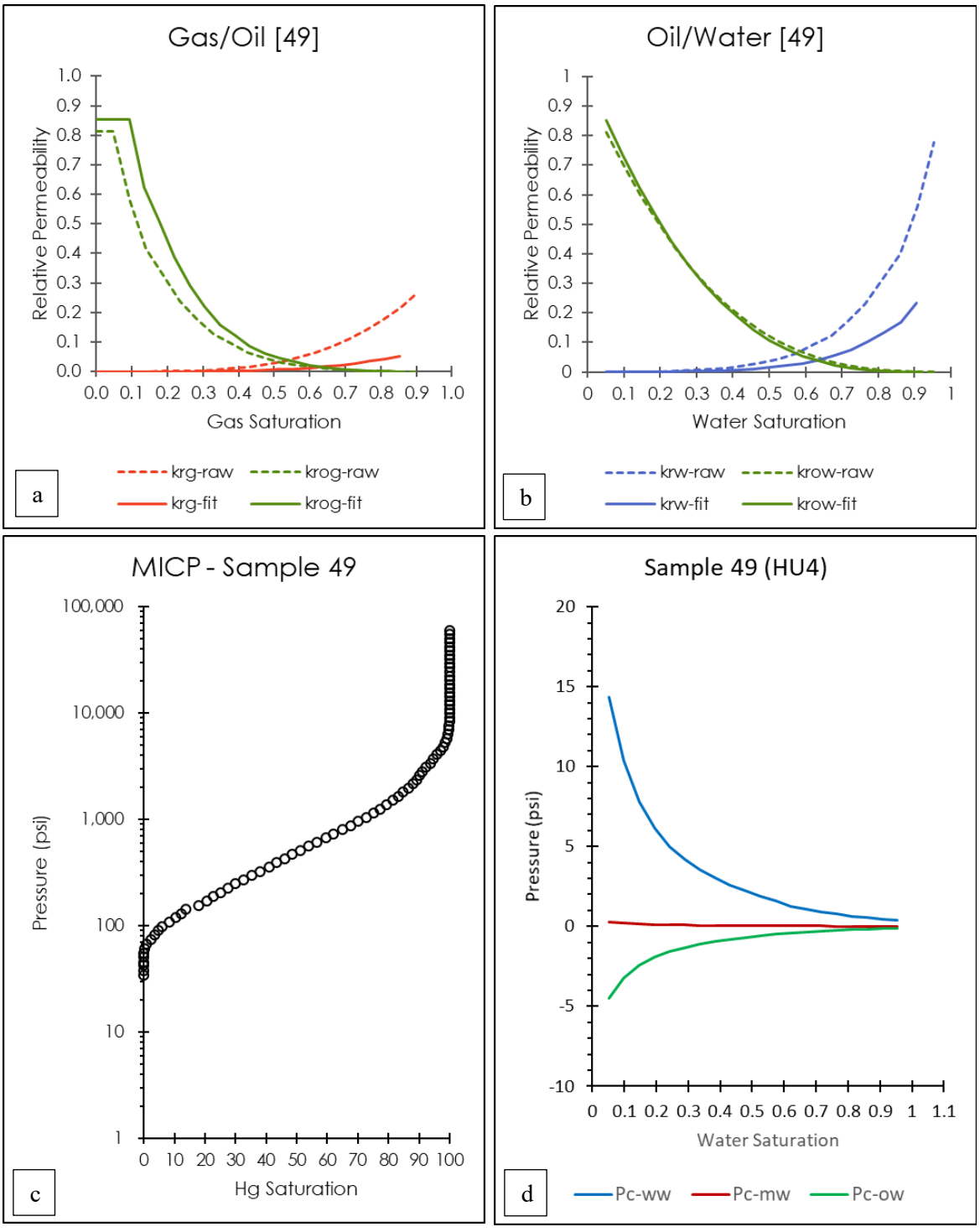

Figure 15 Results of the Pc-to-RP method applied to Sample 49 (HU4), (a) is the gas/oil relative permeability curves (fit and raw), (b) is the oil/water relative permeability curves (fit and raw), (c) is the MICP data, and (d) are the water-wet (ww), mixed-wet (mw), and oil-wet (ow) capillary pressure curves.

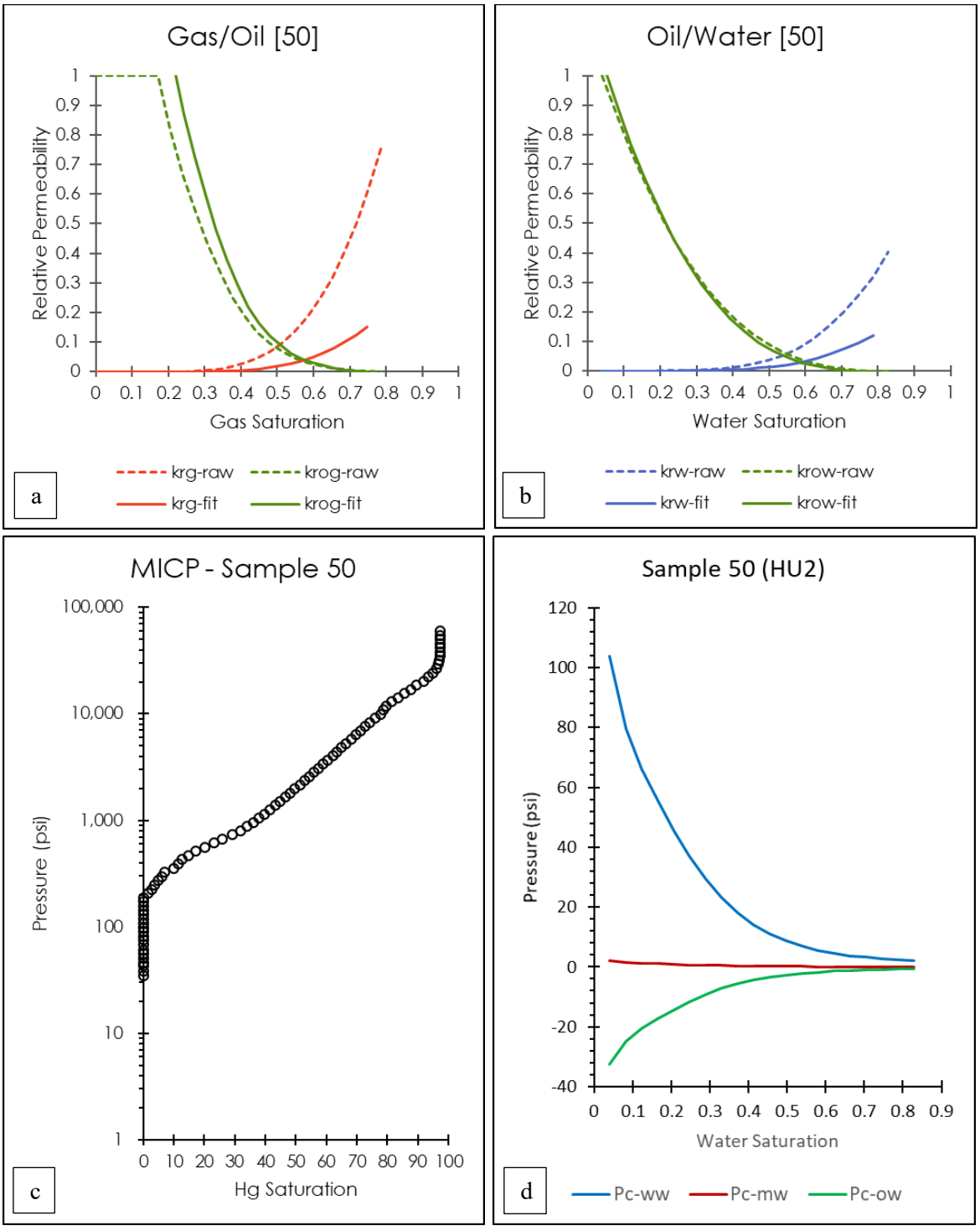

Figure 16 Results of the Pc-to-RP method applied to Sample 50 (HU2), (a) is the gas/oil relative permeability curves (fit and raw), (b) is the oil/water relative permeability curves (fit and raw), (c) is the MICP data, and (d) are the water-wet (ww), mixed-wet (mw), and oil-wet (ow) capillary pressure curves.

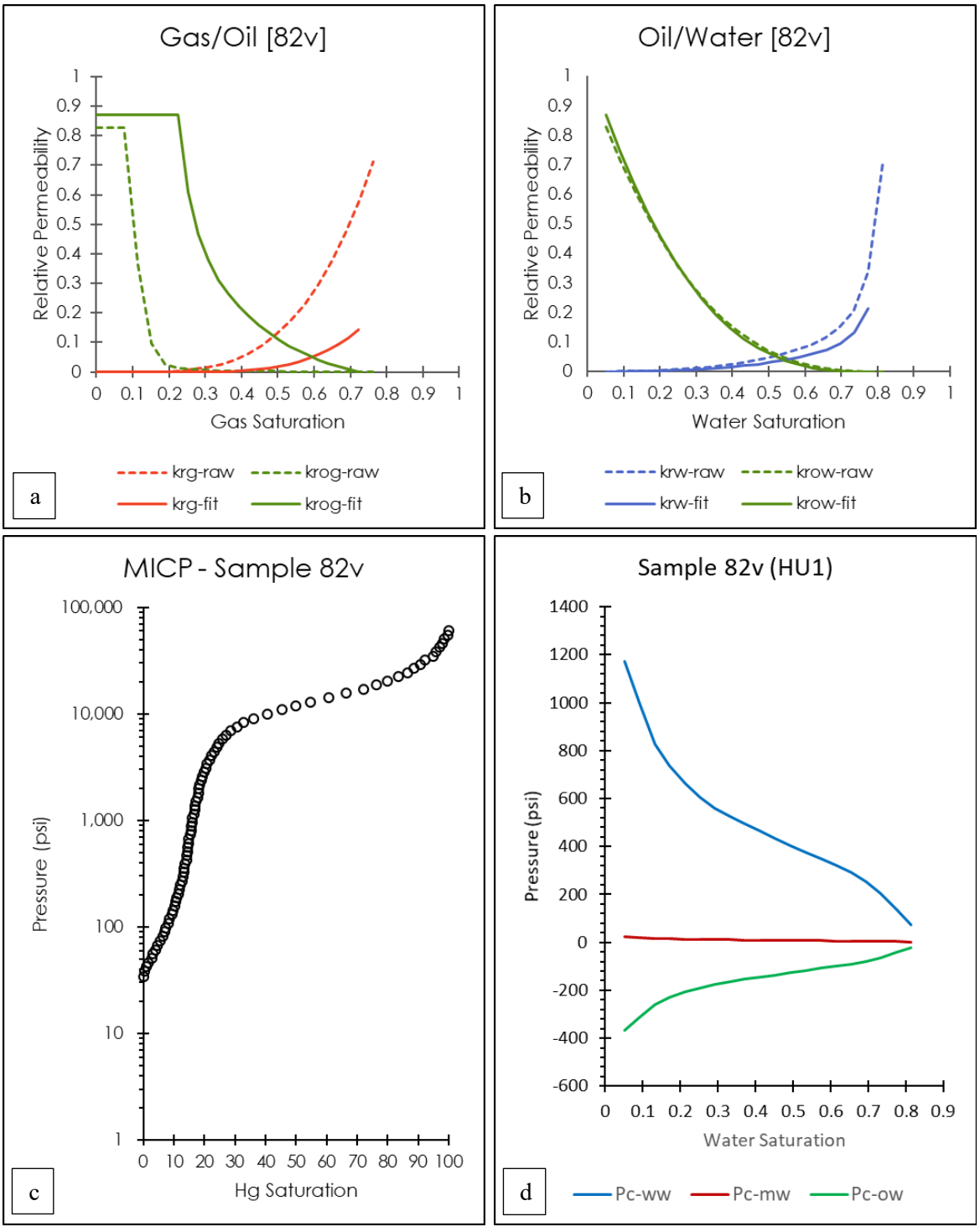

Figure 17 Results of the Pc-to-RP method applied to Sample 82v (HU1), (a) is the gas/oil relative permeability curves (fit and raw), (b) is the oil/water relative permeability curves (fit and raw), (c) is the MICP data, and (d) are the water-wet (ww), mixed-wet (mw), and oil-wet (ow) capillary pressure curves.

9 CONCLUSION

I believe the Pc-to-RP method can increase the resolution of numerical models and overall reservoir characterization by leveraging capillary pressure data to create two- and three-phase relative permeability and capillary pressure relationships. Using this method, you can introduce heterogeneous distribution of relative permeability and capillary pressure linked to discrete hydrostratigraphic units, or other lithologic designations, into the geologic and numerical modeling.

The next step in this research is to use these curves in numerical simulation of the Farnsworth Unit. Both the ‘raw’ and ‘fit curves will need to be used to help understand how predictions change as the critical end-point assumptions change. It may be that the ‘raw’ curves should be used numerical simulation as the ‘up-scaled’ relative permeability. This simulation work is being undertaken as part of the on-going research at Farnsworth by the SWP as part of *Task 7.2.1.3 Relative Permeability Variability* and will be reported on as a final deliverable.

10 REFERENCES

Abbaszadeh, M., Fujii, H., & Fujimoto, F. (1996). Permeability prediction by hydraulic flow units-theory and applications. *SPE Formation Evaluation, 11*(04), 263-271.

Aguilera, R., & Aguilera, M. S. (2001). *The integration of capillary pressures and Pickett plots for determination of flow units and reservoir containers.* Paper presented at the SPE Annual Technical Conference and Exhibition.

Amaefule, J. O., Altunbay, M., Tiab, D., Kersey, D. G., & Keelan, D. K. (1993). *Enhanced reservoir description: using core and log data to identify hydraulic (flow) units and predict permeability in uncored intervals/wells.* Paper presented at the SPE annual technical conference and exhibition.

Baker, L. E. (1988). *Three-Phase Relative Permeability Corrections*. Paper presented at the Enhanced Oil Recovery Symposium, Tulsa, Oklahoma.

Bennion, B., & Bachu, S. (2005). *Relative Permeability Characteristics for Supercritical CO2 Displacing Water in a Variety of Potential Sequestration Zones in the Western Canada Sedimentary Basin*. Paper presented at the SPE Annual Technical Conference and Exhibition, Dallas, TX.

Bennion, B., & Bachu, S. (2006). *The Impact of Interfacial Tension and Pore-Size Distribution/Capillary Pressure Character on CO2 Relative Permeability at Reservoir Conditions in CO2-Brine Systems*. Paper presented at the SPE/DOE Symposium on Improved Oil Recovery, Tulsa, Oklahoma.

Bennion, D. B., & Bachu, S. (2007). Permeability and Relative Permeability Measurements at Reservoir Conditions for CO2-Water Systems in Ultra Low Permeability Confining Caprocks. *SPE International*(SPE Paper # 106995).

Brooks, R. H., & Corey, A. T. (1964). Hydraulic Properties of Porous Media *Hydrology Papers* (Vol. Science and Engineering). Colorado State University.

Burdine, N. T. (1953). Relative permeability calculations from pore size distribution data. *Journal of Petroleum Technology, 5*(03), 71-78.

Chen, X., Kianinejad, A., & DiCarlo, D. A. (2014). *An experimental study of CO2-brine relative permeability in sandstone*.

Corey, A. T. (1954). The interrelation between gas and oil relative permeabilities. *Producers Monthly, 19*(1), 38-41.

Dietrich, J. K., & Bondor, P. L. (1976). Three-Phase Oil Relative Permeability Models. *Society of Petroleum Engineers, 6044*.

Engler, T. W. (2010). Fluid Flow in Porous Media *Petroleum Engineering 524*. New Mexico Tech.

Fan, T., & Grigg, R. (2015). Wettability Measurements of Core Plug from Farnsworth Field. PRRC/New Mexico Tech.

Fatt, I., & Dykstra, H. (1951). Relative permeability studies. *Journal of Petroleum Technology, 3*(09), 249-256.

Firoozabadi, A., & Ramey Jr, H. J. (1988). Surface tension of water-hydrocarbon systems at reservoir conditions. *Journal of Canadian Petroleum Technology, 27*(03).

Gao, Z., & Hu, Q. (2013). Estimating permeability using median pore-throat radius obtained from mercury intrusion porosimetry. *Journal of Geophysics and Engineering, 10*(2).

Gasem, K. A. M., Dickson, K. B., Shaver, R. D., & Robinson Jr, R. L. (1993). Experimental phase densities and interfacial tensions for a CO_2/synthetic-oil and a CO_2/reservoir-oil system. *SPE Reservoir Engineering, 8*(03), 170-174.

Hemmati-Sarapardeh, A., Ayatollahi, S., Ghazanfari, M.-H., & Masihi, M. (2013). Experimental determination of interfacial tension and miscibility of the CO2–crude oil system; temperature, pressure, and composition effects. *Journal of Chemical & Engineering Data, 59*(1), 61-69.

Hocott, C. (1939). Interfacial tension between water and oil under reservoir conditions. *Transactions of the AIME, 132*(01), 184-190.
Honarpour, M. M., Koederitz, L., & Harvey, H. (2018). *Relative permeability of petroleum reservoirs*: CRC press.
Katz, A. J., & Thompson, A. H. (1987). Prediction of rock electrical conductivity from mercury injection measurements. *Journal of Geophysical Research: Solid Earth, 92*(B1), 599-607.
Krevor, S. C., Pini, R., Boxiao Li, & Benson, S. M. (2011). Capillary heterogeneity Trapping of CO2 in a Sandstone Rock at Reservoir Conditions. *Geophysical Research Letters, 38*(15). doi: 10.1029/2001GL048239
Krevor, S. C. M., Pini, R., Zuo, L., & Benson, S. M. (2012). Relative permeability and trapping of CO2 and water in sandstone rocks at reservoir conditions. *Water Resources Research, 48*(2). doi: 10.1029/2011WR010859
Maxey, G. B. (1964). Hydrostratigraphic units. *Journal of Hydrology, 2*, 124-129.
May, R. S. (1987). A numerical simulation study of the Farnsworth Unit waterflood (west side) *Science and Technology Project Report 87-32*. Brea: UNOCAL Corporation.
May, R. S. (1988). A simulation study for the evaluation of tertiary oil recovery by CO2 injection in the Farnsworth Unit *Science and Technology Division Project Report No. 88-37*. Brea: UNOCAL Corporation.
McCaffery, F. G. (1972). Measurement of interfacial tensions and contact angles at high temperature and pressure. *Journal of Canadian Petroleum Technology, 11*(03).
Morrow, N. R. (1990). Wettability and its effect on oil recovery. *Journal of Petroleum Technology, 42*(12), 0149-2136.
Oak, M. J., Baker, L. E., & Thomas, D. C. (1990). Three-Phase Relative Permeability of Berea Sandstone. *Society of Petroleum Engineers, 42*(08), 1054-1061.
Perez-Carrillo, E.-R., Zapata-Arango, J.-F., & Santos-Santos, N. (2008). A New Method For The Experimental Determination of Three-Phase Relative Permeabilities. *Ciencia, Tecnologia y Futuro, 3*(4), 23-43.
Purcell, W. R. (1949). Capillary pressures - Their measurement using mercury and the calculation of permeability therefrom. *Journal of Petroleum Technology, 1*(2), 39-48.
Rasmussen, L., Fan, T., Rinehart, A., Luhmann, A., Ampomah, W., Dewers, T., . . . Grigg, R. (2019). Carbon Storage and Enhanced Oil Recovery in Pennsylvanian Morrow Formation Clastic Reservoirs: Controls on Oil–Brine and Oil–CO2 Relative Permeability from Diagenetic Heterogeneity and Evolving Wettability. *Energies, 12*(19), 3663.
Rose-Coss, D., Ampomah, W., Balch, R. S., Cather, M., Mozely, P., & Rasmussen, L. (2016). An Improved Approach for Sandstone Reservoir Characterization. *SPE International, SPE-180375-MS*.
Rosman, A., & Zana, E. (1977). Experimental studies of low IFT displacement by CO/sub 2/injection: Chevron Research Co.
Stone, H. L. (1970). Probability Model for Estimating Three-Phase Relative Permeability. *Journal of Petroleum Technology, 22*(2), 214-218.
Stone, H. L. (1973). Estimation of Three-Phase Relative Permeability and Residual Oil Data. *Journal of Petroleum Technology, 12*(4), 53-61.
Svirsky, D., Ryazanov, A., Pankov, M., Corbett, P. W., & Posysoev, A. (2004). *Hydraulic flow units resolve reservoir description challenges in a Siberian Oil Field.* Paper presented at the SPE Asia Pacific Conference on Integrated Modelling for Asset Management.
Swanson, B. F. (1978). *A simple correlation between air permeabilities and stressed brine permeabilities with mercury capillary pressures*.
Swanson, B. F. (1981). A simple correlation between permeabilities and mercury capillary pressures. *Journal of Petroleum Technology, 33*(12), 2,498-492,504.

van Genuchten, M. T. (1980). A closed-form equation for predicting the hydraulic conductivity of unsaturated soils. *Soil Science Society of America, 44*(5), 892-898.
Wang, X. (2017). Test Report - NO: RT2017-CUP-UU-06: China University of Petroleum-Beijing.
Ward, J. S., & Morrow, N. R. (1987). Capillary Pressure and Gas Relative Permeabilities of Low Permeable Sandstone. *SPE Formation Evaluation, 13882*.
Webb, P. A. (2001). An introduction to the physical characterization of materials by mercury intrusion porosimetry with emphasis on reduction and presentation of experimental data. *Micromeritics Instrument Corp, Norcross, Georgia*.
Yang, D., & Gu, Y. (2005). Interfacial interactions between crude oil and CO_2 under reservoir conditions. *Petroleum science and technology, 23*(9-10), 1099-1112.
Yang, D., Tontiwachwuthikul, P., & Gu, Y. (2005). Interfacial tensions of the crude oil + reservoir brine + CO2 systems at pressures up to 31 MPa and temperatures of 27 C and 58 C. *Journal of Chemical & Engineering Data, 50*(4), 1242-1249.

11 APPENDIX I

11.1 TWO-PHASE RELATIVE PERMEABILITY AND CAPILLARY PRESSURE CURVES AND DATA

The following two-phase relative permeability and capillary pressure curves were used to develop and calibrate the Pc-to-RP method. These plots below show the curves 'fit' to the laboratory data, used to derive the fitting parameters, and the 'raw' curves developed using the Pc-to-RP method without fitting. Below each relative permeability and capillary pressure chart, the goodness of fit results for each curve of the binary fluid pair, gas(CO_2)/water. The sum of squares analysis (Sum^2) indicates how well the calculated data fit the laboratory data, and the regression analysis provided the R^2 value indicating how correlated the calculated data is to the laboratory data

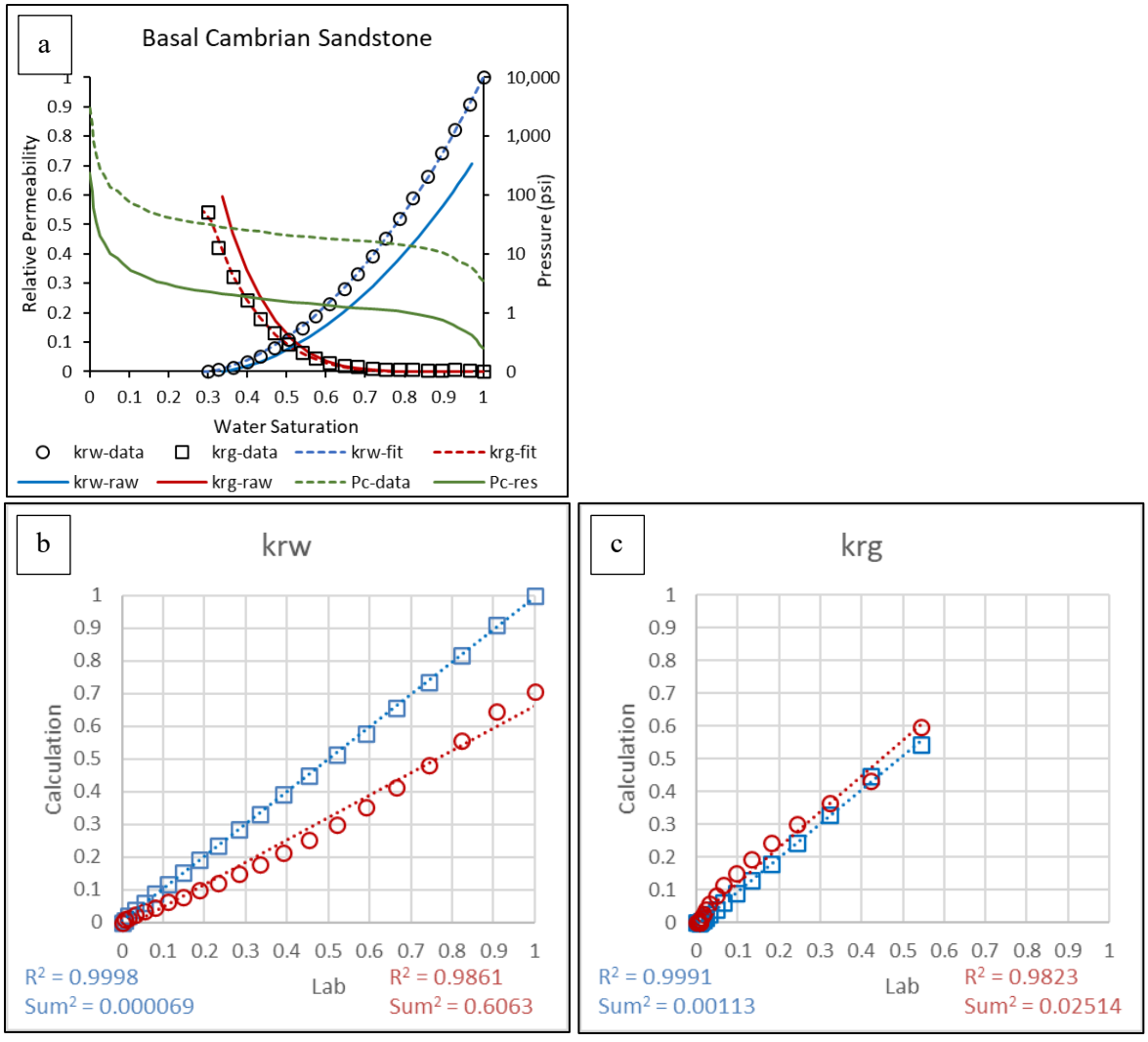

Figure 18 (a) Basal Cambrian Sandstone relative permeability (open symbols) and capillary pressure (green line) measured by Bennion and Bachu (2005, 2006). The blue and red lines are the fitted relative permeability curves using the Pc-to-RP method. Water (b) and CO_2 (c) show the relative permeability regression analysis with the laboratory data plotted on the x-axis and the calculated data on the y-axis.

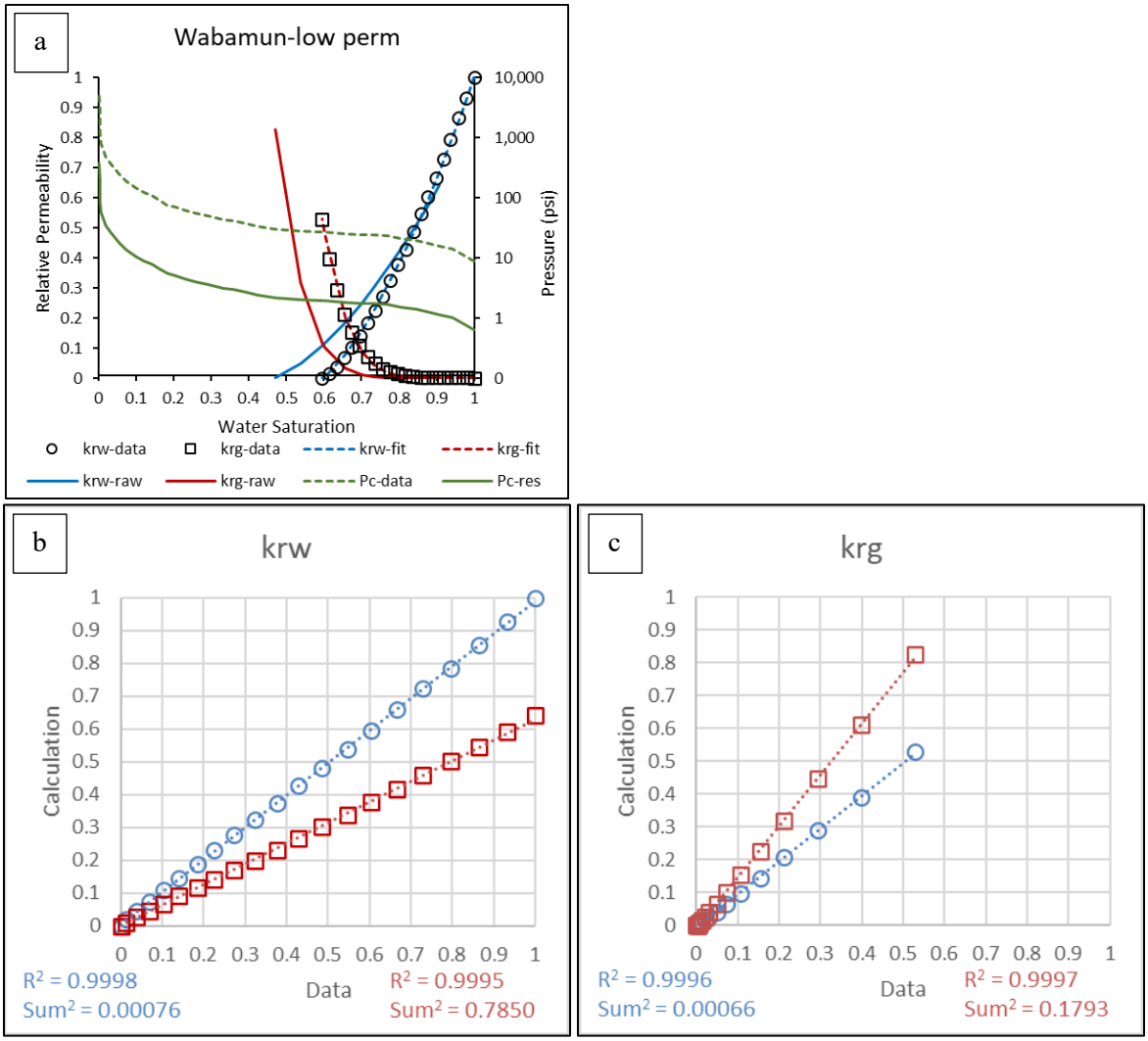

Figure 19 Low permeability sections of the Wabamun Sandstone relative permeability (open symbols) and capillary pressure (green line) measured by Bennion and Bachu (2005, 2006). The blue and red lines are the fitted relative permeability curves using the Pc-to-RP method. Water (b) and CO_2 (c) show the relative permeability regression analysis with the laboratory data plotted on the x-axis and the calculated data on the y-axis.

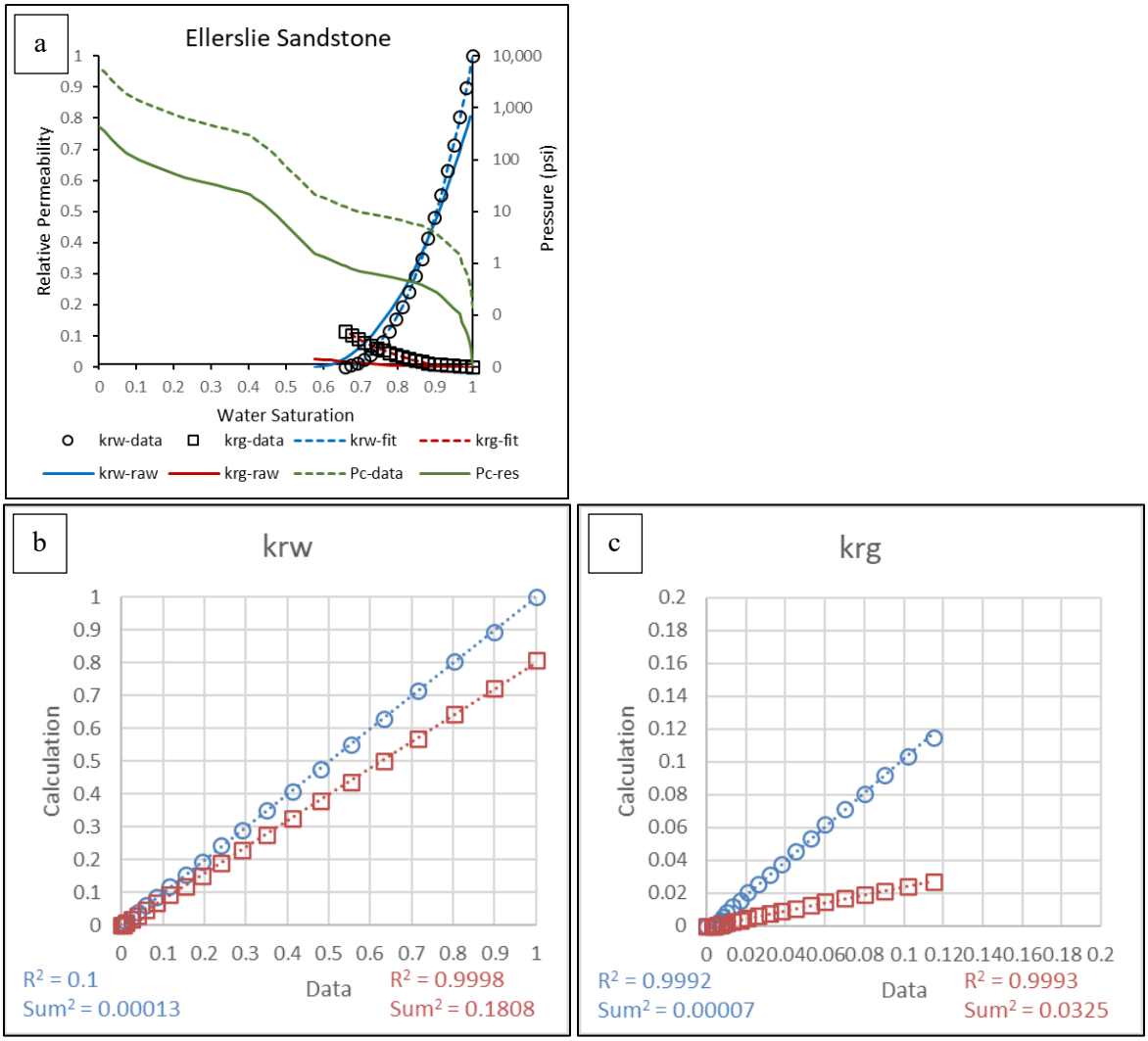

Figure 20 Ellerslie Sandstone relative permeability (open symbols) and capillary pressure (green line) measured by Bennion and Bachu (2005, 2006). The blue and red lines are the fitted relative permeability curves using the Pc-to-RP method. Water (b) and CO_2 (c) show the relative permeability regression analysis with the laboratory data plotted on the x-axis and the calculated data on the y-axis.

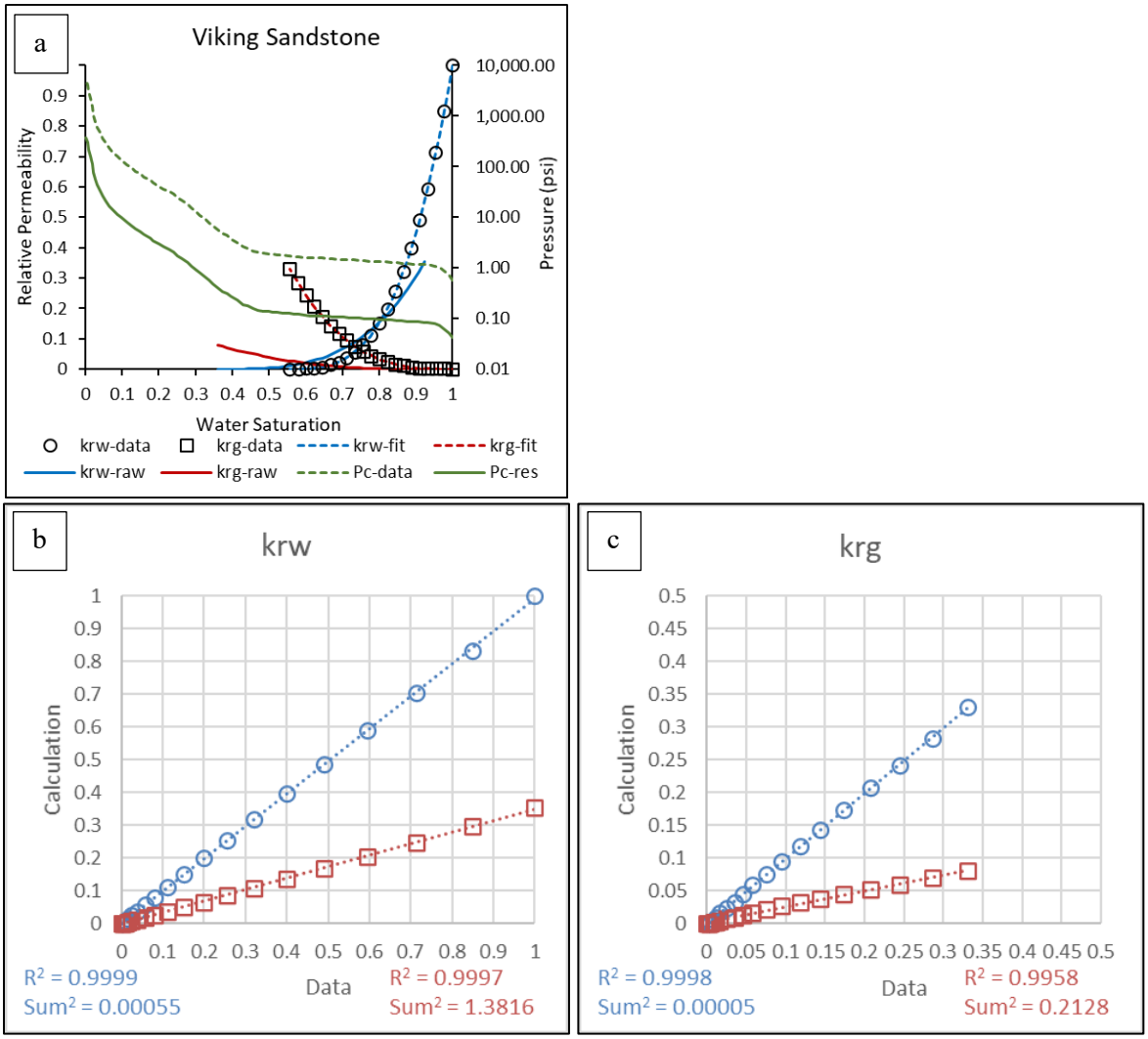

Figure 21 Viking Sandstone relative permeability (open symbols) and capillary pressure (green line) measured by Bennion and Bachu (2005, 2006). The blue and red lines are the fitted relative permeability curves using the Pc-to-RP method. Water (b) and CO_2 (c) show the relative permeability regression analysis with the laboratory data plotted on the x-axis and the calculated data on the y-axis.

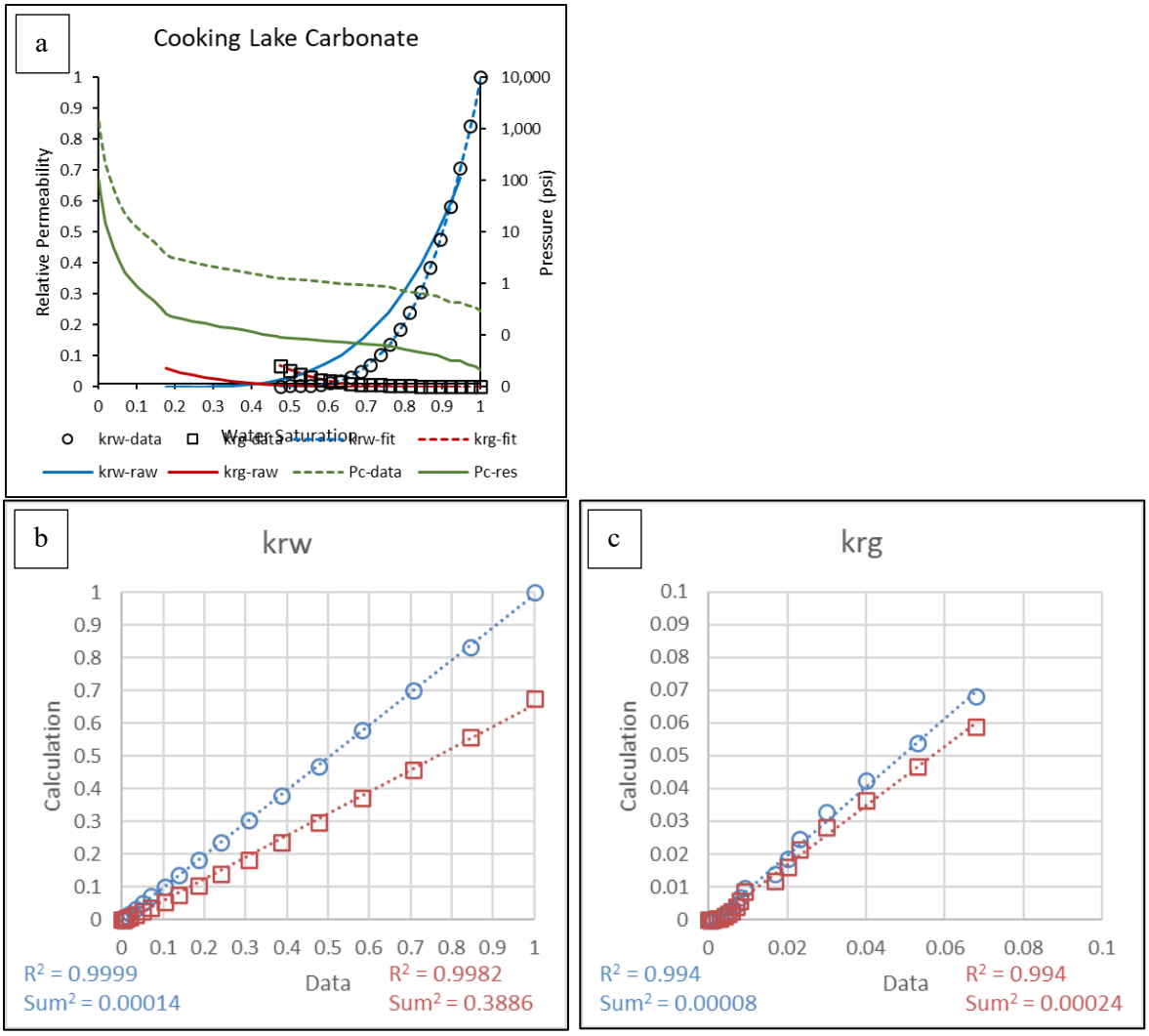

Figure 22 Cooking Lake Carbonate relative permeability (open symbols) and capillary pressure (green line) measured by Bennion and Bachu (2005, 2006). The blue and red lines are the fitted relative permeability curves using the Pc-to-RP method. Water (b) and CO_2 (c) show the relative permeability regression analysis with the laboratory data plotted on the x-axis and the calculated data on the y-axis.

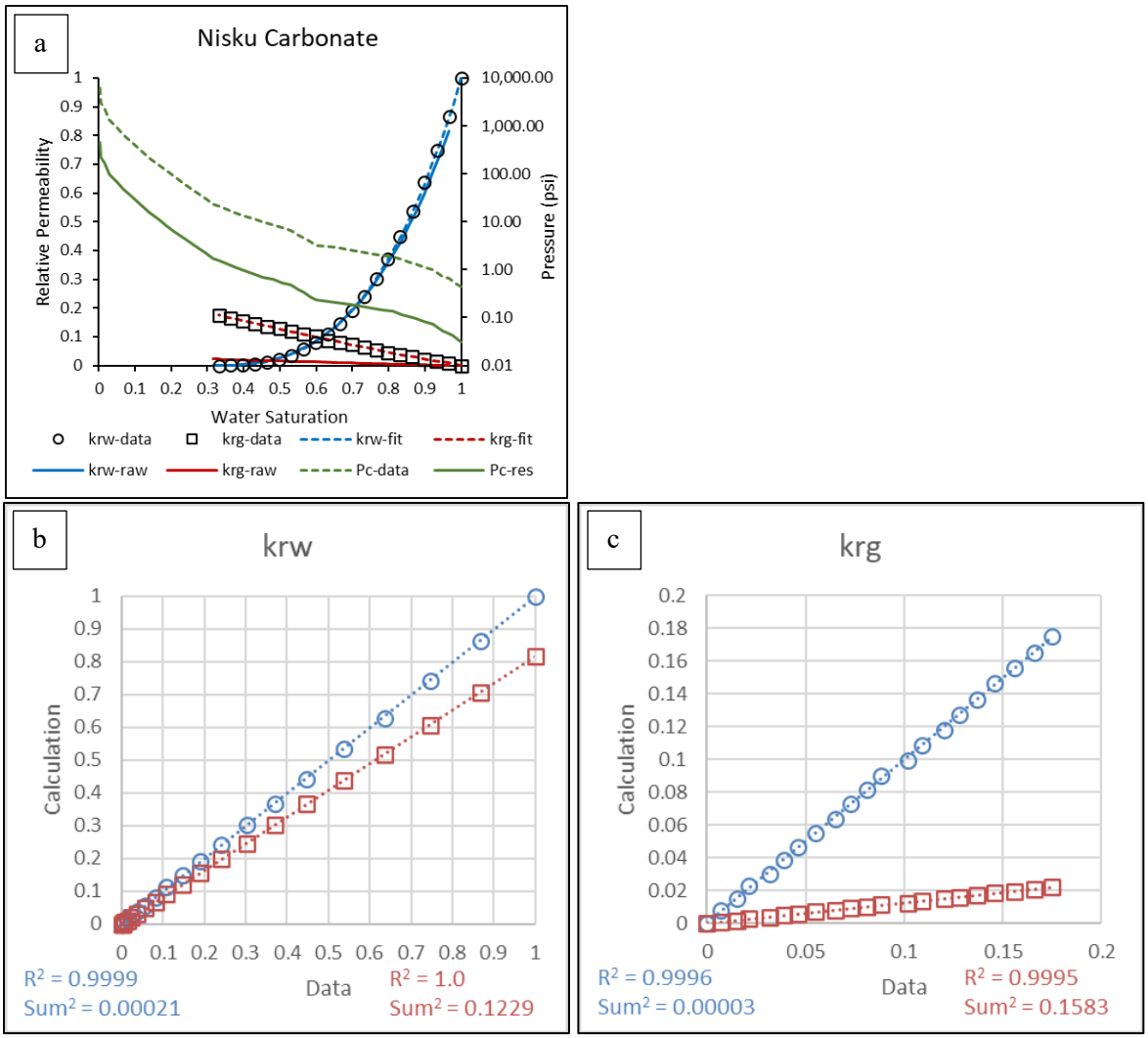

Figure 23 Nisku Carbonate relative permeability (open symbols) and capillary pressure (green line) measured by Bennion and Bachu (2005, 2006). The blue and red lines are the fitted relative permeability curves using the Pc-to-RP method. Water (b) and CO_2 (c) show the relative permeability regression analysis with the laboratory data plotted on the x-axis and the calculated data on the y-axis.

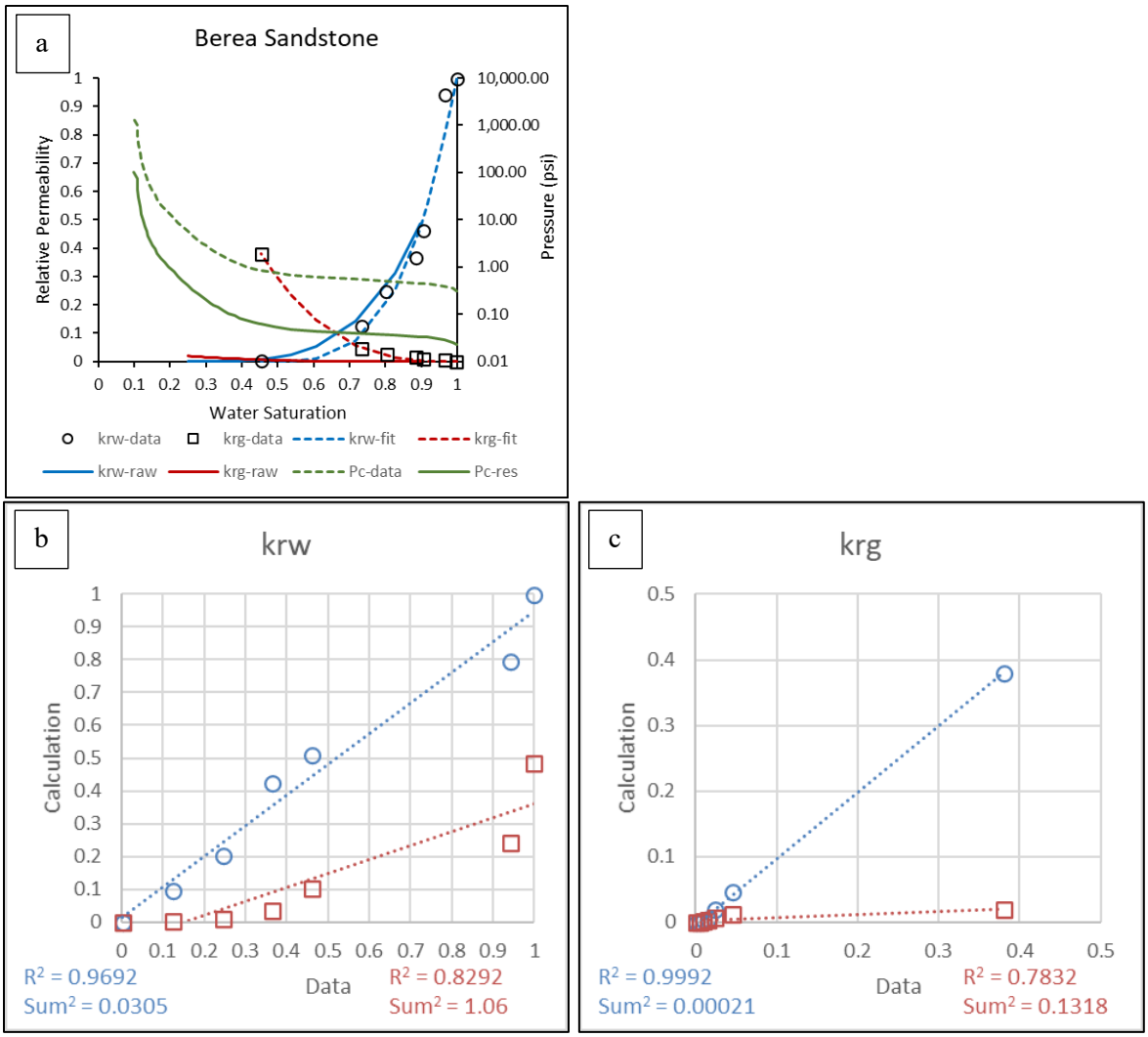

Figure 24 Berea Sandstone relative permeability (open symbols) and capillary pressure (green line) measured by Krevor et al. (2011, 2012). The blue and red lines are the fitted relative permeability curves using the Pc-to-RP method. Water (b) and CO_2 (c) show the relative permeability regression analysis data with the laboratory data plotted on the x-axis and the calculated data on the y-axis.

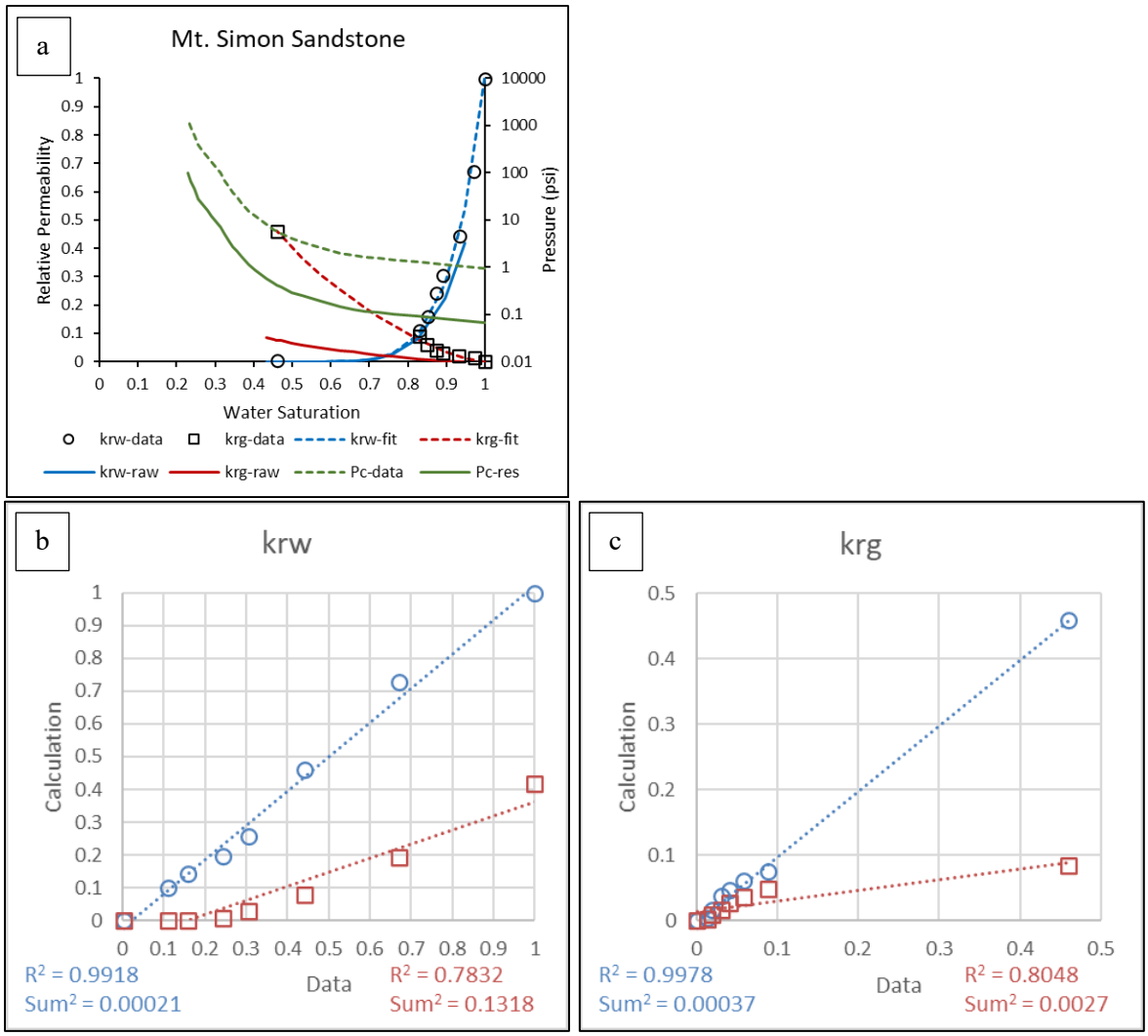

Figure 25 Mt. Simon Sandstone relative permeability (open symbols) and capillary pressure (green line) measured by Krevor et al. (2011, 2012). The blue and red lines are the fitted relative permeability curves using the Pc-to-RP method. Water (b) and CO_2 (c) show the relative permeability regression analysis data with the laboratory data plotted on the x-axis and the calculated data on the y-axis.

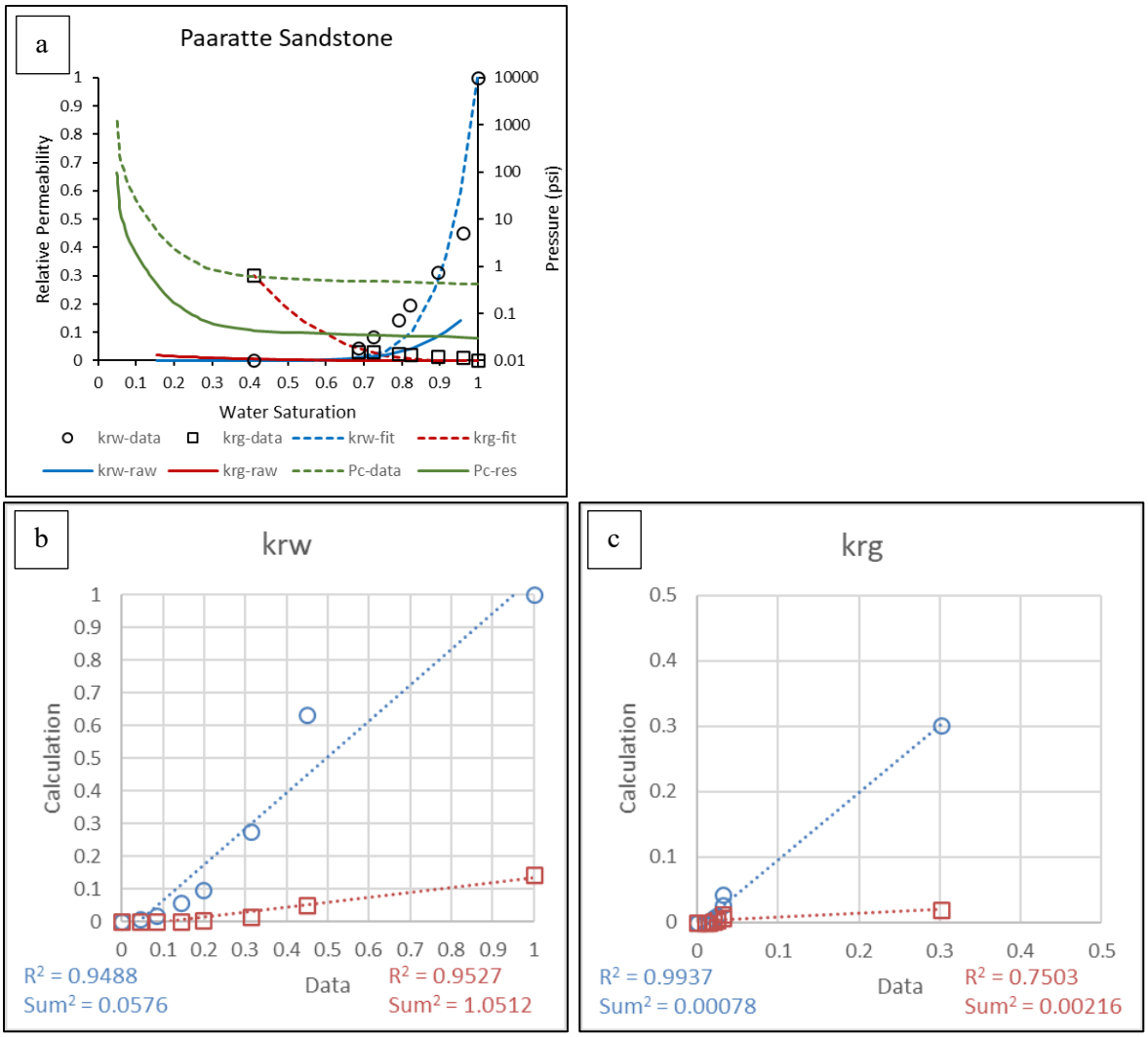

Figure 26 Paaratte Sandstone relative permeability (open symbols) and capillary pressure (green line) measured by Krevor et al. (2011, 2012). The blue and red lines are the fitted relative permeability curves using the Pc-to-RP method. Water (b) and CO_2 (c) show the relative permeability regression analysis data with the laboratory data plotted on the x-axis and the calculated data on the y-axis.

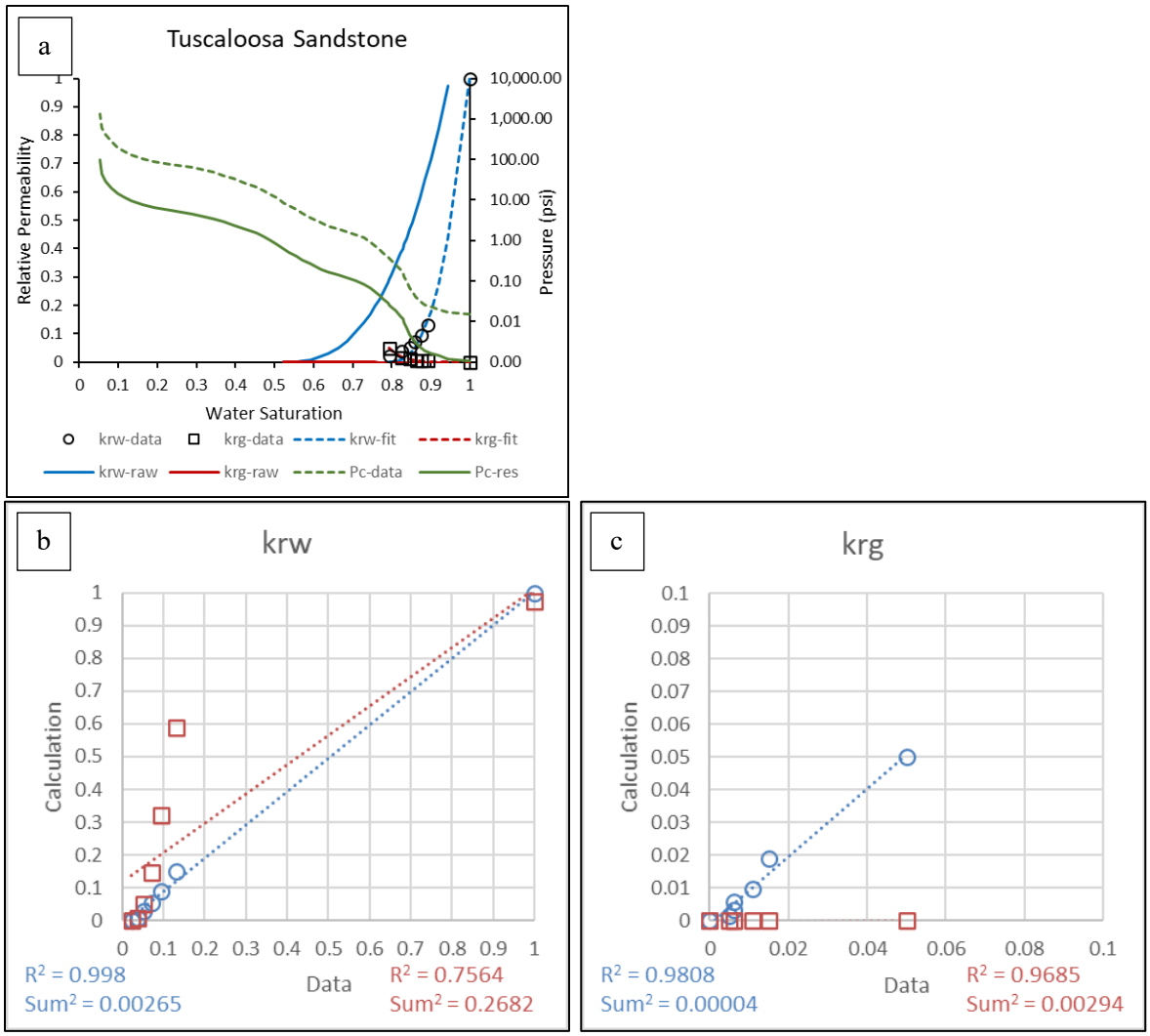

Figure 27 Sandstone relative permeability (open symbols) and capillary pressure (green line) measured by Krevor et al. (2011, 2012). The blue and red lines are the fitted relative permeability curves using the Pc-to-RP method. Water (b) and CO_2 (c) show the relative permeability regression analysis data with the laboratory data plotted on the x-axis and the calculated data on the y-axis.

11.2 Three-Phase Relative Permeability and Capillary Pressure Curves and Data

The following three-phase relative permeability and capillary pressure curves were used in the development and calibration of the Pc-to-RP method. These plots below show the curves 'fit' to the laboratory data, used to derive the fitting parameters, and the 'raw' curves developed using the Pc-to-RP method without fitting. Below each relative permeability and capillary pressure chart, the goodness of fit results for each curve of the binary fluid pairs, gas(CO_2)/oil and oil/water. The sum of squares analysis (Sum^2) indicates how well the calculated data fit the laboratory data. The regression analysis provided the R^2 value indicating how correlated the calculated data is to the laboratory data. The UNOCAL curve in Figure 28 was not fit to MICP data due to the lack of corresponding capillary pressure data.

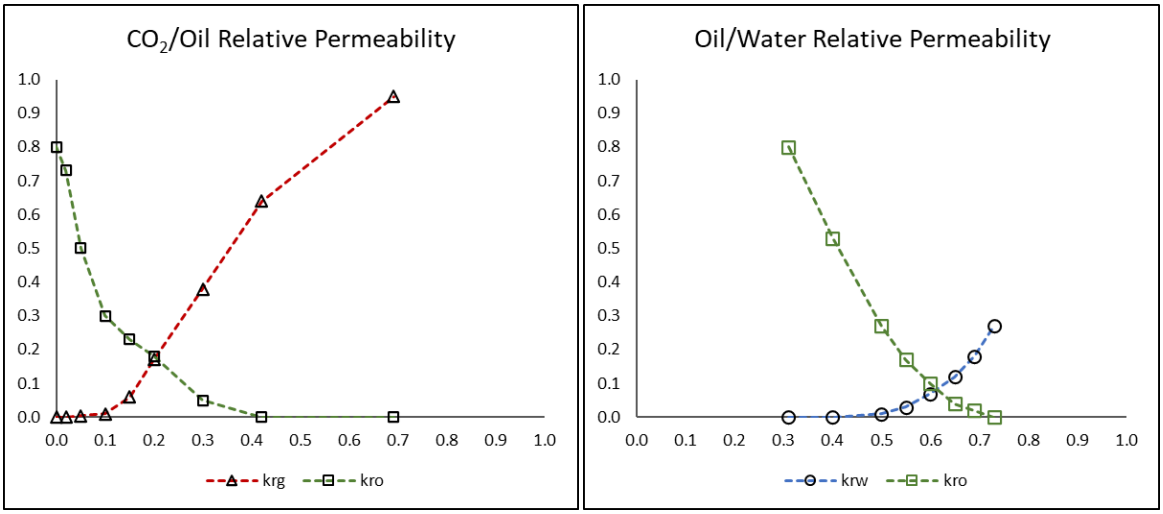

Figure 28 UNOCAL relative permeability curves derived from a study done on the Farnsworth Unit prior to the SWP project (May 1987).

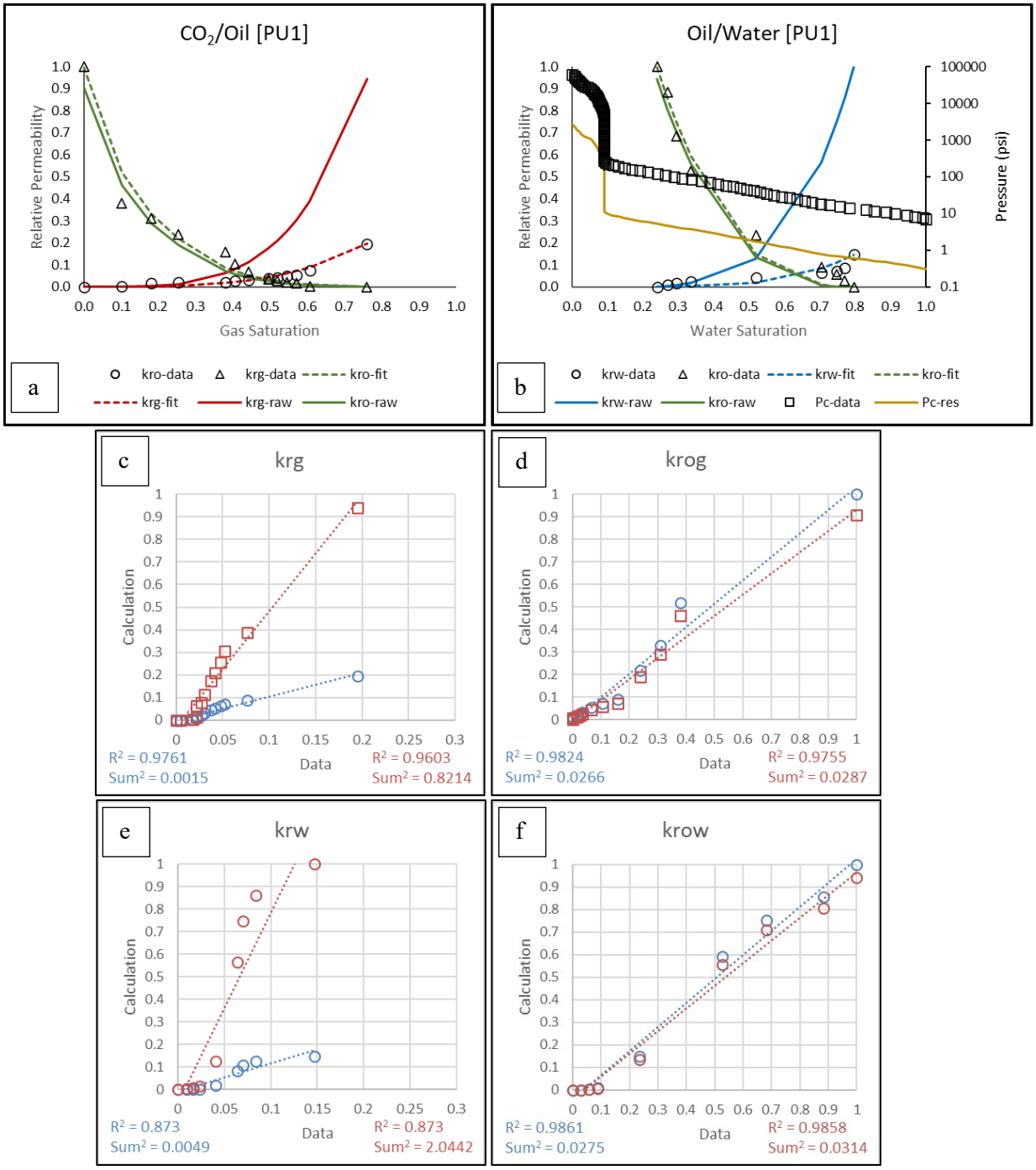

*Figure 29 (a) Wang (2017) relative permeability data Sample 3-7 (gas/oil) and (b) Sample 5-1 (oil/water) along with Sample #58 MICP data plotted as oil/water and gas/oil pairs in open symbols and indicated as *-data on the legend. The dashed lines are the relative permeability curves developed by the Pc-to-RP method fitted to the relative permeability data end-points. The solid lines are the relative permeability curves developed by the Pc-to-RP method without using the relative permeability data end-points. Pc-res curve is the MICP data converted to the reservoir fluid, pressure, and temperature conditions. The four charts (c-f) are the goodness of fit analysis for each curve of the relative permeability relationship showing the laboratory data (x-axis) plotted against the calculated data (y-axis) with the R^2 and sum of squares (Sum^2) values. Blue indicates the 'fit' results, and red the 'raw' results. (c) is the gas (CO_2) in the gas/oil pair, (d) is the oil in the gas/oil pair, (e) is the water in the oil/water pair, and (f) is the oil in the oil/water pair.*

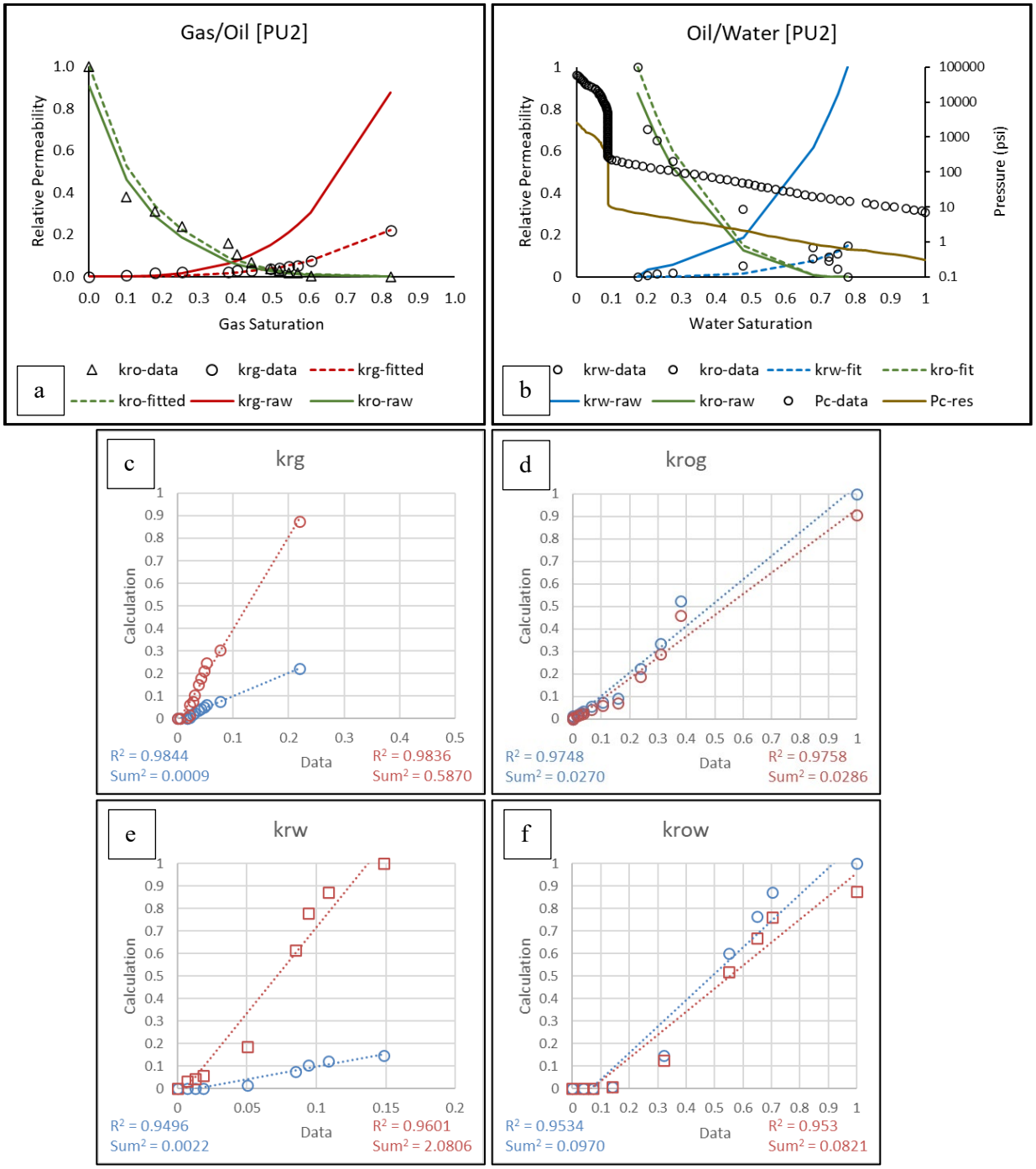

*Figure 30 (a) Wang (2017) relative permeability data Sample 3-7 (gas/oil) and Sample 3-9 (oil/water) along with Sample #58 MICP data plotted as oil/water and gas/oil pairs in open symbols and indicated as *-data on the legend. The dashed lines are the relative permeability curves developed by the Pc-to-RP method fitted to the relative permeability data end-points. The solid lines are the relative permeability curves developed by the Pc-to-RP method without using the relative permeability data end-points. Pc-res curve is the MICP data converted to the reservoir fluid, pressure, and temperature conditions. The four charts (c-f) are the goodness of fit analysis for each curve of the relative permeability relationship showing the laboratory data (x-axis) plotted against the calculated data (y-axis) with the R^2 and sum of squares (Sum^2) values. Blue indicates the 'fit' results, and red the 'raw' results. (c) is the gas (CO_2) in the gas/oil pair, (d) is the oil in the gas/oil pair, (e) is the water in the oil/water pair, and (f) is the oil in the oil/water pair.*

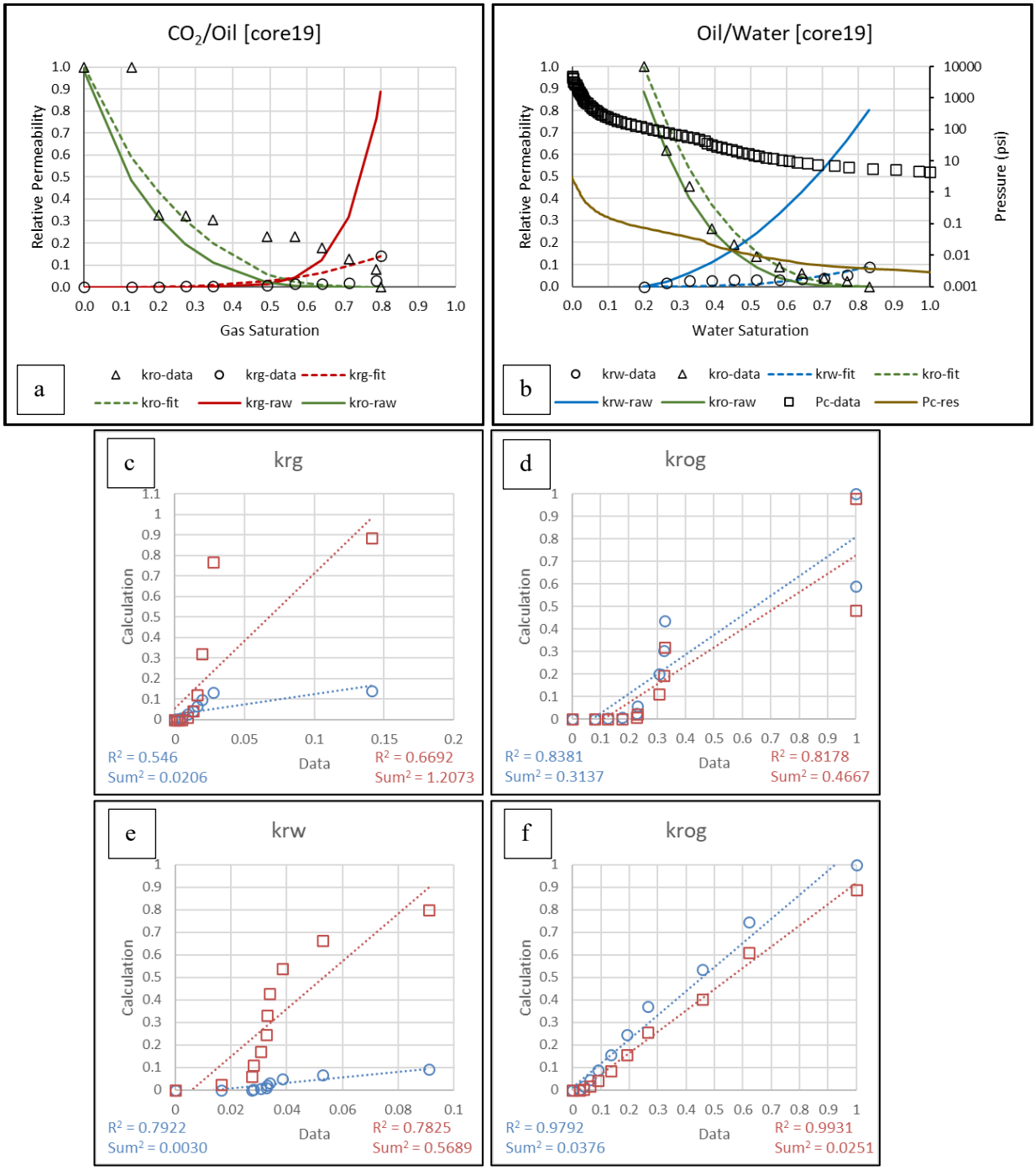

*Figure 31 Rasmussen et al. (2019) relative permeability data Core 19 (gas/oil) and (oil/water) along with Sample #59 MICP data plotted as oil/water and gas/oil pairs in open symbols and indicated as *-data on the legend. The dashed lines are the relative permeability curves developed by the Pc-to-RP method fitted to the relative permeability data end-points. The solid lines are the relative permeability curves developed by the Pc-to-RP method without using the relative permeability data end-points. Pc-res curve is the MICP data converted to the reservoir fluid, pressure, and temperature conditions. The four charts (c-f) are the goodness of fit analysis for each curve of the relative permeability relationship showing the laboratory data (x-axis) plotted against the calculated data (y-axis) with the R^2 and sum of squares (Sum^2) values. Blue indicates the 'fit' results, and red the 'raw' results. (c) is the gas (CO_2) in the gas/oil pair, (d) is the oil in the gas/oil pair, (e) is the water in the oil/water pair, and (f) is the oil in the oil/water pair.*

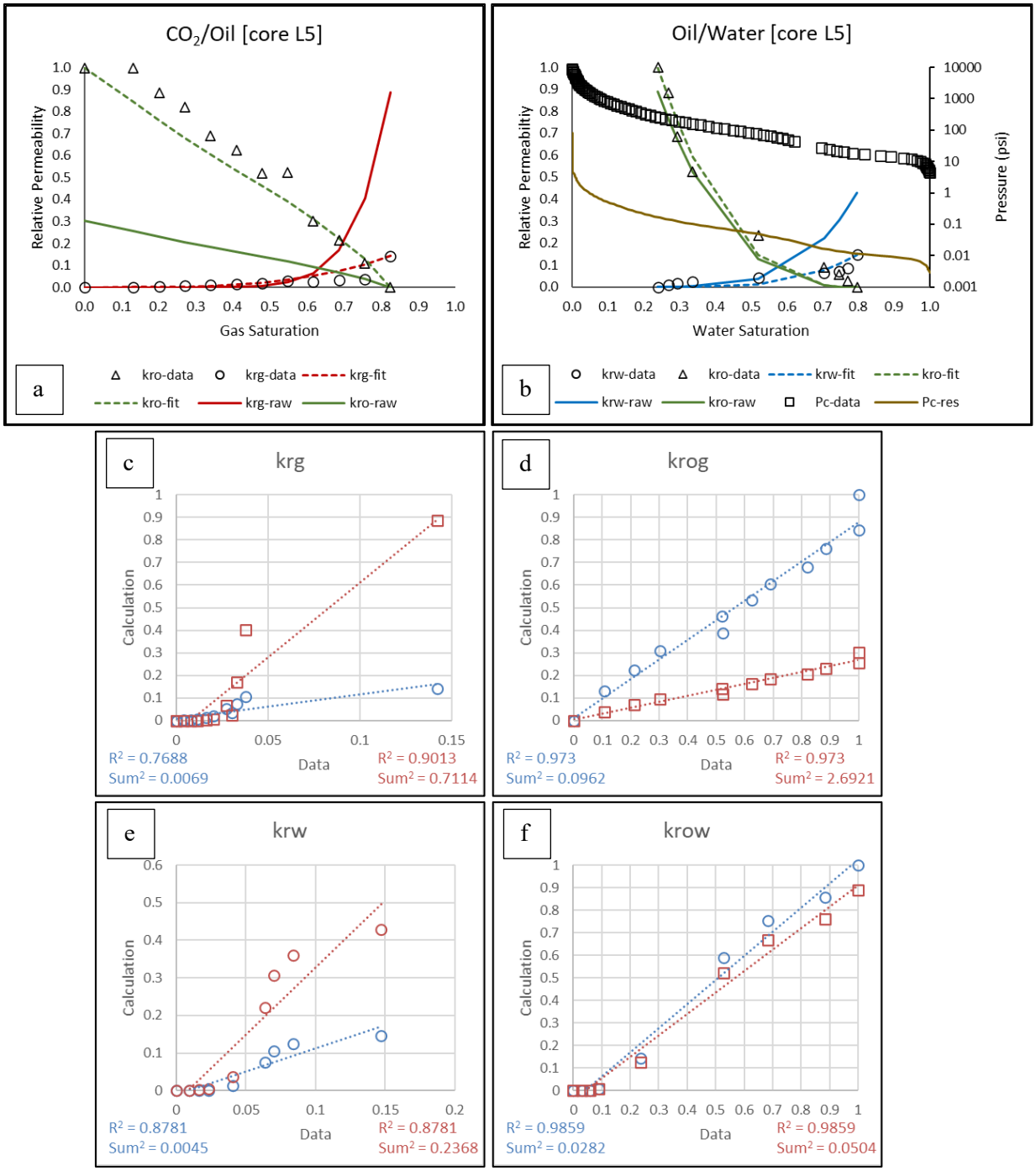

*Figure 32 Rasmussen et al. (2019) relative permeability data Core L5 (gas/oil) (oil/water) along with Sample #57 MICP data plotted as oil/water and gas/oil pairs in open symbols and indicated as *-data on the legend. The dashed lines are the relative permeability curves developed by the Pc-to-RP method fitted to the relative permeability data end-points. The solid lines are the relative permeability curves developed by the Pc-to-RP method without using the relative permeability data end-points. Pc-res curve is the MICP data converted to the reservoir fluid, pressure, and temperature conditions. The four charts (c-f) are the goodness of fit analysis for each curve of the relative permeability relationship showing the laboratory data (x-axis) plotted against the calculated data (y-axis) with the R^2 and sum of squares (Sum^2) values. Blue indicates the 'fit' results, and red the 'raw' results. (c) is the gas (CO_2) in the gas/oil pair, (d) is the oil in the gas/oil pair, (e) is the water in the oil/water pair, and (f) is the oil in the oil/water pair.*